Journal of CO_2 Utilization 24 (2018) 479–499

Contents lists available at ScienceDirect

Journal of CO_2 Utilization

journal homepage: www.elsevier.com/locate/jcou

Pinpointing energy losses in CO_2 plasmas – Effect on CO_2 conversion

Antonin Berthelot*, Annemie Bogaerts

Department of Chemistry, Research group PLASMANT, University of Antwerp, Universiteitsplein 1, 2610 Antwerp, Belgium

ARTICLE INFO

Keywords:
CO_2 conversion
Energy efficiency
Non-equilibrium plasmas
Reduced electric field
Vibrational excitation

ABSTRACT

Plasma technology is gaining increasing interest for CO_2 conversion, but to maximize the energy efficiency, it is important to track the different energy transfers taking place in the plasma. In this paper, we study these mechanisms by a 0D chemical kinetics model, including the vibrational kinetics, for different conditions of reduced electric field, gas temperature and ionization degree, at a pressure of 100 mbar. Our model predicts a maximum conversion and energy efficiency of 32% and 47%, respectively, at conditions that are particularly beneficial for energy efficient CO_2 conversion, i.e. a low reduced electric field (10 Td) and a low gas temperature (300 K). We study the effect of the efficiency by which the vibrational energy is used to dissociate CO_2, as well as of the activation energy of the reaction $CO_2 + O \rightarrow CO + O_2$, to elucidate the theoretical limitations to the energy efficiency. Our model reveals that these parameters are mainly responsible for the limitations in the energy efficiency. By varying these parameters, we can reach a maximum conversion and energy efficiency of 86%. Finally, we derive an empirical formula to estimate the maximum possible energy efficiency that can be reached under the assumptions of the model.

1. Introduction

Since the beginning of the industrial revolution, a large part of the world's energy production is based on processes involving the combustion of fossil fuels. These processes release the carbon contained in the fuels into the atmosphere in the form of CO_2, thus giving rise to an alarming increase of the atmospheric CO_2 concentration. It is now widely accepted that the anthropogenic CO_2 emissions are responsible for the increase of the surface temperature on Earth [1]. Hence, there is a growing interest into various methods to find alternative, renewable energy sources. These energy sources typically have an important drawback: the intermittency of their power generation. Therefore, over the last few years, large research efforts have been directed towards finding solutions for energy storage. One of these methods, the conversion of CO_2 into value-added compounds, has recently received a great interest [2–4]. For instance, the conversion of CO_2 to CO (and oxygen), followed by conversion into hydrocarbons through the Fischer–Tropsch process, would be an interesting way to store energy via a carbon-neutral process. Plasma technology could be suitable for this process, because it uses electricity, and can easily be switched on/off, thus allowing to store intermittent electrical energy. It was indeed shown that low-temperature non-equilibrium plasmas can be an energy-efficient way to dissociate CO_2 [5,2]. In such plasmas, the electrons acquire a much higher temperature than the heavy particles (e.g. the gas molecules), so they can activate the gas by electron impact excitation, ionization and dissociation, without the need to heat the entire gas. This enables endothermic reactions to occur at low temperature, thus keeping the energy cost lower than in a thermal process [5]. This is naturally an interesting property in the framework of energy storage.

The most common types of discharges studied for CO_2 conversion are microwave (MW) plasmas [6–10], gliding arc (GA) plasmas [11–13] and dielectric barrier discharges (DBD) [14–17], although other plasma types are being investigated as well, such as ns-pulsed discharges [18,19], spark discharges [20] and atmospheric glow discharges [21].

While MW and GA plasmas offer relatively high energy efficiencies in most lab-experiments, the energy efficiency of DBDs remains rather low. One the main differences between MW and GA plasmas on the one hand, and DBDs on the other hand, is the value of the electron temperature, which tends to be higher in a DBD [22]. This electron temperature results from the reduced electric field (i.e. electric field divided by gas density), which is indeed higher in a DBD than in a MW and GA plasma [2,23].

The commonly accepted explanation to this lower energy efficiency in a DBD is that a higher electron temperature favors dissociation of CO_2 by direct electron impact from the ground state. This process requires more energy than strictly needed for dissociation, as it results in the creation of electronically excited O atoms. On the other hand, at low electron temperature, characteristic for MW and GA plasmas, it would be possible, through electron impact vibrational excitation and

* Corresponding author.
E-mail address: antonin.berthelot@uantwerpen.be (A. Berthelot).

https://doi.org/10.1016/j.jcou.2018.02.011
Received 11 December 2017; Received in revised form 2 February 2018; Accepted 18 February 2018

vibrational pumping, to climb the vibrational energy ladder of CO_2, until the dissociation energy is reached, which is much more energy efficient [2,5,22–24]. This phenomena is also described in other gases, such as H_2, N_2 and CO [25].

Evidence shows, however, that both MW and GA plasmas, in most experiments, especially at atmospheric pressure, are in close-to thermal equilibrium [10,26,27,13]. Indeed, the vibrational distribution function (VDF) follows a Boltzmann distribution, and is thus not overpopulated at the highest levels, needed for efficient dissociation. Thus, MW and GA plasmas at atmospheric pressure are not taking full advantage of the possibilities offered by non-equilibrium, that are characteristic for plasma.

Over the last few years, the research on CO_2 plasma kinetics modeling has been focusing on finding ways to enhance the energy efficiency of the CO_2 plasma by achieving a better understanding of the underlying processes leading to dissociation, and in particular vibrational excitation.

Pietanza and coworkers [28–33] focused on the coupling between the electron energy distribution function (EEDF) and the CO_2 plasma kinetics, as well as the different dissociation mechanisms. Recently, they further investigated the CO kinetics in a state-to-state model [34]. In our group, we have focused on the key role of vibrational excitation in a CO_2 plasma and its influence on the plasma kinetics and energy efficiency of CO_2 conversion in MW and GA plasma vs DBDs [22,26,27,35–39].

Furthermore, Ponduri et al. [40] developed a time-dependent 1D model to describe the conversion of CO_2 in a DBD. Grofulović et al. [41] proposed a new set of cross sections for CO_2 plasmas. This set was validated from the comparison between swarm data obtained by solving Boltzmann equation and available experimental data. The role of the electron impact dissociation cross-section was further investigated in our group [42].

More recently, following the method of Turner [43–45], and in continuation of the work of Koelman et al. [46] on the verification of the rate coefficients used in our CO_2 kinetics model, we have also investigated how the uncertainties present on the measurements of the rate coefficients can affect the outputs of the model [47]. We have found that the uncertainty on certain important calculation results, such as the CO_2 conversion, can reach up to 100%. However, this study also revealed that the trends predicted by the model are typically not very affected by the uncertainty on the rate coefficient data, implying that this type of modeling should focus on trends rather than on absolute values.

In the present work, we investigate, using a 0D chemical kinetics model, the way in which energy transfers take place inside the plasma. Indeed, energy efficiencies reported for plasma-driven CO_2 conversion reach up to 90% for a MW plasma operating with a supersonic flow [5,6], where the plasma is formed in the low pressure zone of the flow. Modeling, on the other hand, has only reached energy efficiencies in the vicinity of 30% at best [22,26]. The record energy efficiencies of the early experiments carried out in the former Soviet Union [5,6] have not been reproduced since then. However, energy efficiencies reaching up to 48% have been reported in experiments carried out recently at DIFFER [9]. Therefore, we want to check which energy losses might be present in the model, and/or which processes limit the theoretical energy efficiency. This should allow us to understand the limitations to energy efficient CO_2 conversion, both in the model and in general.

Therefore, we use conditions that were found to be ideal for CO_2 conversion in our previous work [26]. In continuation of our work on the uncertainties of the rate coefficients, we investigate here also the effect of the parameters chosen in the scaling laws on dissociation reaction rate coefficients, as well as the effect of the activation energy of the reaction $CO_2 + O \rightarrow CO + O_2$, as these two parameters are expected to limit the energy efficiency of CO_2 conversion.

Furthermore, to investigate the effect of different plasma operating conditions on energy efficient CO_2 conversion, we also consider different values of the reduced electric field, as well as different gas temperatures and different ionization degrees. These correspond to the parameters that can be improved by optimizing the design of the discharge setup. Some of these conditions might be difficult to currently reproduce experimentally, but can be considered as recommendations towards future experiments.

The paper is organized as follows. In Section 2, the model is described, as well as the chemistry set considered. The results are shown in Section 3. In Section 3.1, the CO_2 conversion and energy pathways are analyzed for different conditions of reduced electric field, gas temperature and ionization degree. Section 3.2 is dedicated to the verification of the rate coefficients and scaling laws used for the two main neutral dissociation reactions, to elucidate their effect on the calculated CO_2 conversion and energy efficiency. Section 3.3 attempts to define a general expression for the maximum energy efficiency that can be obtained with plasma. Finally, conclusions are given in Section 4.

2. Model description

2.1. Chemistry set

Table 1 lists the species taken into account in this work. The chemistry set considered here is the same as in our previous work, following kinetic data literature verification [47]. A rather small set is used here, compared to the model of Refs. [36,22,26], because these species and reactions are found to play the dominant role, and adding more (minor) species and (minor) reactions increases the uncertainty on the results and does not lead to a better accuracy, while increasing computation time.

The model takes into account the asymmetric mode vibrational levels of CO_2 up to the dissociation limit, as well the first 4 symmetric mode vibrational levels and the first 10 vibrational levels of CO. It was found in our previous research [37] that the higher vibrational levels of CO do not make a significant difference to the models result.

The list of reactions included in the model is shown in Appendix A. Tables A.1 and A.2 present the list of electron impact reactions

Table 1
Species described in the model.

Neutral ground states	CO_2	CO	O_2	O	$C_{(g)}$
Standard formation enthalpy [48] [eV]	−4.08	−1.15	0	2.58	7.43

Charged species
CO_2^+, CO^+, CO_4^+, O^-, O_2^-, CO_3^-, CO_4^-, e^-

Excited states	Associated energy [eV]	State[a]
$O_2[v_{1-4}]$	Anharmonic oscillator	
$CO[v_{1-10}]$	Anharmonic oscillator	
$CO_2[v_{1-21}]$	Anharmonic oscillator	(00n)
$CO_2[v_a]$	0.083	(010)
$CO_2[v_b]$	0.167	(020) + (100)
$CO_2[v_c]$	0.252	(030) + (110)
$CO_2[v_d]$	0.339	(040) + (120) + (200)
$CO_2[e_1]$	10.5	$(^1\Sigma_u^+)$ + $(^3\Pi_u)$ + $(^1\Pi_u)$
$O_2[e_1]$	0.98	$(a^1\Delta_g)$ + $(b^1\Sigma_g^+)$
$O_2[e_2]$	8.4	$(B^3\Sigma_u^-)$ + higher triplet states
$CO[e_1]$	6.22	$(a^3\Pi_r)$
$CO[e_2]$	7.9	$(A^1\Pi)$
$CO[e_3]$	13.5	$(a'^3\Sigma^+)$ + $(d^3\Delta_i)$ + $(e^3\Sigma^-)$ + $(b^3\Sigma^+)$
$CO[e_4]$	10.01	$(C^1\Sigma^+)$ + $(E^1\Pi)$ + $(B^1\Sigma^+)$ + $(I^1\Sigma^-)$ + $(D^1\Delta)$

[a] CO_2 electronic states designation from Grofulović et al. [41], O_2 and CO electronic states notation from Huber and Herzberg [49].

considered, described by cross-section data and analytical rate coefficients, respectively. Tables A.3 and A.4 show the reactions involving ions, and neutral molecules and atoms, respectively, while Table A.5 lists the reactions consisting in energy transfers between the molecules considered.

2.2. Scaling laws

The rate coefficients and cross sections used for the various reactions considered in this work are typically only known for reactions involving ground state molecules, and not for vibrationally excited molecules. We follow here the procedure developed by Kozák and Bogaerts [36], using scaling laws to determine the various rate coefficients. The reactions involving vibrational levels can be grouped in three categories: electron impact reactions (Table A.1 in Appendix A), vibrational energy exchanges (vibrational–vibrational (VV) and vibrational–translational (VT), Table A.5 in Appendix A) and neutral reactions (Table A.4 in Appendix A). For the electron impact reactions, Fridman's approximation [5] is used to obtain the electron impact cross sections. For VV and VT reactions, the SSH theory [50,51] is used. More information can be found in Kozák and Bogaerts [36]. Finally, vibrational excitation can also lower the activation energy of a reaction between two neutral molecules. To scale the neutral reactions with vibrational energy, we use the following formula, expressed in the framework of the so-called theoretical-informational approach [5,52]:

$$k(T_g, E_v) = A.\ \min\left[\exp\left(-\frac{E_a - \alpha E_v}{T_g}\right), 1\right] \quad (1)$$

where E_a is the activation energy, E_v is the vibrational energy of the molecule, α is a parameter determining the efficiency of the vibrational energy to help overcoming the activation energy barrier, varying between 0 and 1 depending on the reaction, and T_g is the gas temperature. Eq. (1) implies that a vibrationally excited molecule reacting in a dissociation reaction 'sees' an activation energy of $E_a - \alpha E_v$, instead of simply E_a. Then, in order to overcome the activation energy barrier of a reaction, in conditions of negligible thermal energy (i.e. low gas temperature T_g), a molecule needs to have an energy $E_v \gtrsim E_a/\alpha$. In this case, the reaction can be considered barrierless and its rate coefficient becomes equal to the pre-exponential factor A in Eq. (1).

The values of α considered here are given in Table A.4 (in Appendix A). Except for reaction N1 (see Table A.4 in Appendix A), these values are calculated based on the Fridman–Macheret approximative α model [5]:

$$\alpha = \frac{E_a}{2E_a - \Delta H°} \quad (2)$$

Eq. (2) shows that α, i.e. the efficiency of vibrational energy to overcome the activation energy barrier, depends only on the activation energy and the enthalpy of a reaction. It is close to 1, i.e. maximum efficiency, for endothermic reactions with an activation energy close to their enthalpy. An endothermic reaction with a high activation energy $E_a >> \Delta H°$ will have an α close to 0.5. Only exothermic reactions can have an α below 0.5 and α is 0 for barrierless exothermic reactions.

Note that in the case of reaction N1 (see Table A.4 in Appendix A), an endothermic CO_2 dissociation reaction, the activation energy determined experimentally (E_a(N1) = 4.53 eV) is lower than the reaction enthalpy (5.52 eV), which is a theoretical minimum. This is probably due to the difficulty to experimentally determine the rate coefficient of this reaction with a high energy barrier, especially at low gas temperatures.

To avoid this anomaly, and since Eq. (2) obviously does not take this case into consideration, we use a value $\alpha_M = 0.82$ instead of using Eq. (2). This value is derived from $E_a(\text{N1}) - \alpha_M E_v = 0$, taking $E_v = \Delta H°(\text{N1})$. This choice of α_M ensures that CO_2 molecules with a vibrational energy equal to the enthalpy of the reaction see no activation energy barrier for reaction N1.

Hence, this way, we ensure that only the molecules with vibrational energies equal to or higher than the enthalpy of the reaction can effectively react through reaction N1 in the absence of significant translational energy. Using a value of α_M above 0.82 (i.e. closer to 1) may result in lack of energy conservation, since it would allow CO_2 molecules with vibrational energies similar to the activation energy (i.e. below the reaction enthalpy) to react, without the need to provide extra thermal (translational) energy. This will be explained in more detail in Section 3.2.1.

As also explained in Section 3.2.1, the model is quite sensitive to the value of α_M. Note that in theory, α_M should be close to one with $E_a(\text{N1}) \simeq \Delta H°(\text{N1})$. More experimental investigation is thus required to verify this rate coefficient and in particular its activation energy.

In Section 3.2.1, we will investigate the effect of the α parameters of the two main dissociation reactions (N1 and N2, see Table A.4 in Appendix A) on the calculated CO_2 conversion and energy efficiency and the underlying mechanisms, in order to find out the maximum theoretical energy efficiency that the model can predict for various conditions. Likewise, in Section 3.2.2, we will discuss the effect of the activation energy linked with the α parameter of reaction N2 on the calculation results.

2.3. Plasma model

We used the code ZDPlasKin [53] to develop a zero-dimensional chemical kinetics model. The densities of all species n_s are solved as a function of time using:

$$\frac{dn_s}{dt} = \sum_j [a_{sj}^R - a_{sj}^L] k_j \prod_l n_l \quad (3)$$

a_{sj}^R and a_{sj}^L are the right- and left-hand side stoichiometric coefficients of species s, respectively. k_j is the rate coefficient of reaction j. $\prod_l n_l$ is the product of the densities n_l of species present on the left side of reaction j.

The system of differential equations is solved using the so-called DVODE solver [54], which is included within the ZDPlasKin code [53].

The electron energy distribution function (EEDF) is calculated using the Boltzmann solver Bolsig+ [55] and the set of cross sections presented in Table A.1 (in Appendix A). Superelastic collisions are also included. In order to keep the calculation time reasonable, the EEDF is only updated when the electron density changes by more than 3% or if the reduced electric field or the density of the other species change more than 0.1%. The EEDF is used to calculate the (energy dependent) rate coefficients of the various electron impact reactions (see Table A.1 and A.2 in Appendix A). The rate coefficients of the other (so-called heavy particle) reactions are either constant or depend on the gas temperature, and they are adopted from literature, as indicated in Tables A.3–A.5 (in Appendix A).

The model starts at $t = 0$ with pure CO_2, and a Boltzmann vibrational distribution. At $t = 0$, the plasma starts with a given DC reduced electric field E/N (where E is the electric field and N is the gas number density). The power density applied to the plasma is simply calculated using Joule's law $P = \sigma E^2 = N^2(E/N)^2\sigma$, where σ, the conductivity, is given by $\sigma = e n_e \mu_e$. μ_e is the electron mobility, obtained from the Boltzmann solver, and e is the elementary charge. The electron density n_e in the plasma is fixed to a value determined by the ionization degree α_i: $n_e = N\alpha_i$. The plasma stops when the power applied to the gas has reached a specific energy input (SEI) value of 2 eV/molec. The SEI is calculated as the ratio between energy input density and gas number density.

In the experiments, typical SEI values range from 0.1 to 10 eV/molec [9]. An SEI of 2 eV/molec coupled to a high conversion yields a high energy efficiency, since in theory a minimum of 2.93 eV is required to dissociate one CO_2 molecule under standard conditions (see Eq. (7)).

We keep the gas temperature T_g and pressure p constant throughout the whole simulation. We perform calculations for 300 K, 1000 K and 2000 K so that we can study more in detail the effect of gas temperature

on the various reaction mechanisms. Moreover, it is known that a low gas temperature (in the order of 300 K) is required to have a significant vibrational over-population and a better energy efficiency [22,26], as will also be discussed below.

The effect of pressure on the reaction kinetics was studied in our previous work [26]. We chose here a fixed pressure of 100 mbar, as it is representative for MW plasma experiments yielding a good energy efficiency [6,10,9] and it allows us to study non-equilibrium phenomena [26].

Note that plasmas for CO_2 conversion often operate at atmospheric pressure as well, but they typically give rise to lower energy efficiency, due to either negligible vibrational kinetics (like in DBD [36]) or a VDF too close to thermal equilibrium (like in MW or GA plasmas [26]). Therefore, atmospheric pressure is less suitable to study the non-equilibrium phenomena, and to pinpoint the energy transfers in the plasma in order to predict the maximum theoretical energy efficiency.

Ionization degrees α_i between 10^{-6} and 10^{-4} are considered here. The typical value of α_i in a CO_2 MW or GA plasma is indeed around 10^{-6} [56,10], while it can reach up to 10^{-4} in some DBD setups [42]. n_e is fixed to a very low value ($\alpha_i = 10^{-16}$) outside of the plasma zone, in order to ensure that no power is deposited there.

2.4. Calculated CO_2 conversion and effect of gas expansion

The ideal gas law is applied at all times, and because pressure and temperature are kept constant, the total species number density stays constant as well:

$$N = \sum_s n_s = \frac{p}{k_b T_g} \tag{4}$$

where k_b is the Boltzmann constant.

It is thus possible to express the SEI as a function of time since the beginning of the plasma, Δt, and as a function of the input variables which were defined before:

$$\mathrm{SEI} = \int_0^{\Delta t} \frac{P}{N}\mathrm{d}t = \int_0^{\Delta t} (E/N)^2 \mu_e e \alpha_i \left(\frac{p}{k_B T_g}\right)^2 \mathrm{d}t \tag{5}$$

Moreover, one CO_2 molecule dissociates in several smaller molecules and radicals (e.g. CO and O or $\frac{1}{2}O_2$), and this yields gas expansion [57]. In order to account for this gas expansion in the model, we simply introduce a variable $\beta(t)$, the gas expansion factor, initially equal to 1, and which evolves with time, due to the gas expansion. For example, if all CO_2 is dissociated and forms CO and $\frac{1}{2}$ O_2, then $\beta = \frac{2}{3}$, since $\frac{3}{2}N_0$ molecules are formed (with N_0 the initial CO_2 density). Hence, the CO_2 conversion is calculated as:

$$X(t)[\%] = \left[1 - \frac{n_{CO_2}(t)}{\beta(t) N_0}\right] \times 100\% \tag{6}$$

where n_{CO_2} is the total CO_2 density (i.e. sum of ground state and all vibrational and electronically excited levels).

We will mostly present the calculated CO_2 conversion at the end of the simulation, i.e. 10 ms after the end of the plasma. Indeed, after 10 ms, most of the radicals will have recombined at the pressure considered here, and the gas will be close to chemical equilibrium.

The energy efficiency η of the CO_2 conversion is calculated using the enthalpy of the reaction $CO_2 \rightarrow CO + \frac{1}{2}O_2$ at 300 K, $\Delta H^\circ = 2.93$ eV/molec:

$$\eta[\%] = X[\%]\frac{\Delta H^\circ}{\mathrm{SEI}} \tag{7}$$

where SEI is the specific energy input (kept constant at 2 eV/molec in these simulations; cf above).

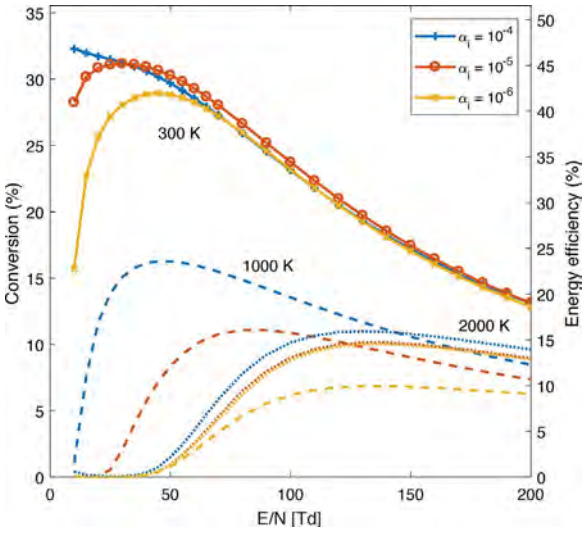

Fig. 1. CO_2 conversion (left *y*-axis) and corresponding energy efficiency (right *y*-axis) as a function of the reduced electric field *E/N*, for three different ionization degrees (10^{-6}, 10^{-5}, 10^{-4} in blue, orange and yellow, respectively) and three different gas temperatures (300 K, 1000 K, 2000 K, shown with full lines, dashed lines and dotted lines, respectively.) (For interpretation of the references to color in this figure legend, the reader is referred to the web version of this article.)

3. Results and discussion

3.1. CO_2 conversion and energy transfers in the plasma

3.1.1. Calculated CO_2 conversion and energy efficiency

Fig. 1 shows the CO_2 conversion (left *y*-axis) and corresponding energy efficiency (right *y*-axis) as a function of the reduced electric field *E/N* for different gas temperatures (300 K, 1000 K and 2000 K) and different ionization degrees α_i for an SEI of 2 eV/molec. The energy efficiency is calculated based on the energy acquired by the electrons from the electric field: the energy necessary to heat the gas is not taken into account here. Thus the energy efficiency is here more an indicative value, since the gas temperature is not self-consistently calculated. Note that at gas temperatures of 2000 K and below, purely thermal conversion is a negligible process [2,13]. A rise in gas temperature within this range actually has a detrimental effect on the conversion, as discussed below. Note that the calculation of the gas temperature in a 0D model is always subject to uncertainties due to the presence of strong gradients of gas temperature and the heat losses due to convection, conduction and radiation, which can hardly be included in this type of model. The heat due to losses of the power can be easily obtained from the energy efficiency: the vast majority of the energy not going to conversion (i.e. chemical bonds) goes to heat in the end.

It should also be realized, as pointed out in our previous study [47], that the uncertainty on the conversion predicted by the model can be substantial and therefore, the focus should be on trends rather than on absolute values. The absolute values of various quantities (CO_2 conversion and energy efficiency, relative contribution to dissociation, etc.) presented in this paper should be considered as an indication of the differences caused by a change of conditions.

At $T_g = 300$ K, and $\alpha_i = 10^{-5}$ or $\alpha_i = 10^{-6}$, the CO_2 conversion reaches a maximum value of 31% and 29% for an *E/N* of 30 Td and 45 Td, respectively. On the other hand, with $\alpha_i = 10^{-4}$, the CO_2 conversion decreases monotonously with *E/N*, reaching up to 32% for an *E/N* of 10 Td. Above 50 Td, the differences between different ionization degrees become negligible. At 200 Td, the CO_2 conversion has dropped to about 13% for all ionization degrees.

At $T_g = 1000$ K and with $\alpha_i = 10^{-6}$, the CO_2 conversion increases with *E/N*, from zero at 40 Td to approximately 7% at *E/N* = 100 Td and above. At $\alpha_i = 10^{-5}$ and $\alpha_i = 10^{-4}$ a maximum conversion of 11% at 90 Td and 16% at 50 Td is reached, respectively.

Finally, at $T_g = 2000$ K, the CO_2 conversion shows a similar behavior for all values of α_i, although $\alpha_i = 10^{-4}$ gives a slightly higher conversion. The CO_2 conversion starts increasing from around 50 Td to reach a maximum around 130 Td, and slowly decreases for $E/N > 150$ Td. For high values of E/N, a gas temperature of 2000 K with an ionization degree above 10^{-5} can give slightly higher conversion than at 1000 K.

To link these values to the experiments, note that MW and GA discharges typically operate at E/N values of 100 Td and below, while DBDs typically operate at 200 Td and above [2,23]. It is however difficult to sustain a plasma with low values of E/N (50 Td and below), since attachment reactions are more important than ionization reactions at low E/N, due to the difference in the energy threshold of the two cross sections [58,59]. Nevertheless, it is possible to work around this, by using two different energy sources: one with a large E/N (ionization source) and one with a lower E/N, as shown in a CO_2 plasma by Andreev et al. [60].

In general, the conversion drops drastically upon higher gas temperature, while a higher ionization degree is beneficial for the conversion. The effect of E/N depends on the value of the gas temperature. These trends will be explained in more detail in the next sections.

The energy efficiency follows exactly the same behavior as the conversion, which is logical from Eq. (7) as the SEI is kept constant. It is a factor 1.46 higher than the conversion (i.e. ΔH°/SEI = 2.93/2.0). Thus, the highest energy efficiency reached at these conditions is 45%, at 300 K, $E/N = 10$ Td and $\alpha_i = 10^{-4}$.

In literature a wide range of energy efficiencies has been reported, depending on the type of discharge and the setup [2]. DBD plasmas typically have energy efficiencies of 15% or below [61,62,16], which corresponds well to the energy efficiencies predicted here at high E/N, i.e. values typical of DBDs. MW and GA plasmas, on the other hand, reach higher energy efficiencies. Values of η up to 90% have been reported in literature from the former USSR in supersonic flow MW plasmas [6], while most recent experiments give values up to 50% for MW plasmas [9,10] and GA plasmas [13,12]. The experimental maximum energy efficiencies thus correspond to the highest values obtained here (Fig. 1), or are even slightly higher, although they were typically not obtained at ideal conditions, while the conditions presented here are somehow optimal, and thus higher values of energy efficiency would be expected from the model.

Therefore, the following two sections, 3.1.2 and 3.1.3, focus on the energy transfers taking place within the plasma, in order to explain the results shown in Fig. 1. The theoretical limitations of the energy efficiency in the model will also be discussed below.

3.1.2. Time-dependent behavior of the energy transfers in the plasma

In this section, we first show the electron energy loss mechanisms as a function of time and for various conditions. Indeed, the energy from the electric field will in first instance entirely go to the electrons. The electrons then redistribute this energy to the other particles, through various processes. Vibrational excitation is known as the key to high energy efficiencies and thus we will later focus on the CO_2 vibrational energy transfer mechanisms. The goal is to investigate how much of the plasma power effectively goes into CO_2 dissociation and to identify the energy loss mechanisms for various conditions.

Fig. 2 shows the electron energy losses in the plasma for a gas temperature of 300 K, an ionization degree of 10^{-6} and a reduced electric field of 50 Td (Fig. 2a) and 150 Td (Fig. 2b). The electron energy losses are normalized to the maximum value of the energy applied to the electrons. Note that the energy losses due to elastic collisions between electrons and neutrals are included in the model, but are several orders of magnitude lower than the inelastic energy losses, at the conditions considered here. The time dependent CO_2 conversion is plotted against the right y-axis. Note that the overall time dependent CO_2 conversion after the plasma may be slightly lower than the CO_2 conversion at the end of the simulation (plotted in Fig. 1) due to the back reaction N4 (see Table A.4 in Appendix A) occurring after the plasma due to the presence of O atoms.

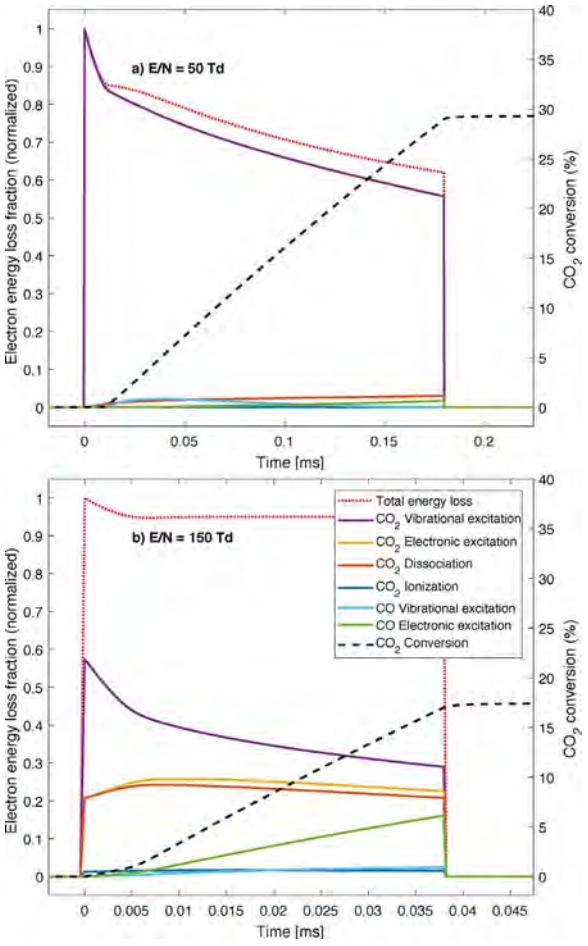

Fig. 2. Electron energy loss fractions (left y-axis) and CO_2 conversion (right y-axis) as a function of time for a gas temperature of 300 K, an ionization degree of 10^{-6}, a pressure of 100 mbar and a reduced electric field of 50 Td (panel a, top) and 150 Td (panel b, bottom). The energy losses are normalized to the maximum of the total energy applied to the electrons. (For interpretation of the references to color in this figure citation, the reader is referred to the web version of this article.)

In general, the electron energy pathways are mainly determined by the value of E/N and the gas chemical composition. Gas temperature and ionization degree have thus only an indirect effect. Therefore, the results are only shown for one gas temperature and one value of the ionization degree.

At $E/N = 50$ Td, by far the dominant electron energy loss is CO_2 vibrational excitation, accounting for more than 90% of the electron energy losses. The other energy losses only contribute for a few %.

At $E/N = 150$ Td, CO_2 vibrational excitation is still the main electron energy loss, and accounts for 58% of the losses at the beginning of the plasma and 32% at the end of the plasma. However, CO_2 electronic excitation and dissociation are also significant energy losses, accounting for between 21% and 26%. Furthermore, CO electronic excitation also becomes increasingly important as energy loss process as time evolves, i.e. due to the increasing CO density (upon conversion of CO_2), and it contributes for up to 15%.

The difference between 50 and 150 Td is explained by the average electron energy, which is about 0.9 eV at 50 Td and about 2.6 eV at 150 Td. As this is the average electron energy, there are of course electrons with higher energy in the tail of the distribution. Still, at 50 Td, there are not many electrons with sufficient energy to overcome the large thresholds of electronic excitation and dissociation reactions (i.e. 10.5 eV and 7 eV, respectively). On the other hand, at 150 Td, there

is a competition between different processes. Moreover, the vibrational excitation cross sections show a maximum at relatively low electron energies (0.38 eV for $CO_2 + e \rightarrow CO_2\nu_1 + e$), which means that the chance to transfer the electron energy to vibrational levels will decrease with increasing electron energy.

The total energy lost by the electrons to inelastic collisions varies with time, although E/N and n_e are fixed, which may seem counter-intuitive. However, the electron energy loss mechanisms also depend on the gas composition. Therefore, at the beginning there is a sharp peak of electron energy loss, due to the lack of superelastic collisions at the beginning of the plasma, which can be explained from the time required for the population of vibrationally excited states to build up. Once their concentration is higher, they release back part of their energy to the electrons through superelastic collisions, which decreases the total electron energy loss. Moreover, in Fig. 2a, we see that the electron energy loss decreases continuously with time. This is caused by the increasing CO concentration, as the electrons lose their energy more easily to CO_2 than to CO. This also leads to a higher electron temperature over time (from 0.65 eV at the very beginning of the plasma to 1.05 eV at the end) since the electrons will thus store more energy. Indeed, the electron temperature is more or less inversely proportional to the total electron energy loss.

It is also interesting to note that CO vibrational excitation is not an important energy loss mechanism, despite the relatively high CO concentrations at the end of the plasma (i.e. molar concentrations up to 25% for a conversion of 29% at 50 Td). This is due to the important energy transfer between the vibrational levels of CO_2 and CO (reaction V8, Table A.5 in Appendix A). This creates a large vibrationally excited CO population, giving rise to important superelastic CO vibrational excitation reverse reactions (i.e. vibrational deexcitation), which almost entirely compensate for the forward reactions. This behavior is of course only significant with large CO_2 vibrational populations and high CO concentrations (i.e. E/N of 50 Td or below and gas temperature of 300 K).

The results shown in Fig. 2 are representative for other conditions as well, since the electron energy loss mechanisms almost only depend on the value of E/N and the gas composition, in particular the CO density. Therefore, the results for other conditions of ionization degree and gas temperature are very similar, with the exception of the energy losses to CO that depend, of course, on the CO density. The behavior of the electron energy losses as a function of E/N is described in more detail below.

As can be concluded Fig. 2, vibrational excitation is the main electron energy loss mechanism. It is therefore interesting to see where the energy stored in the CO_2 vibrational levels of CO_2 effectively goes, and in particular how much of it effectively goes to CO_2 dissociation.

Fig. 3 shows the main vibrational energy loss processes for a reduced electric field of 50 Td, an ionization degree of 10^{-6} and a gas temperature of 300 K (Fig. 3a) and 1000 K (Fig. 3b). The vibrational losses are calculated from the balance of vibrational energy before and after the reaction. These losses are normalized to the maximum energy that the vibrational levels received from the electrons (i.e. purple curve in Fig. 2a, for the $T_g = 300$ K case). Note that the sum of the energy losses by the individual processes must not be equal to the vibrational energy received from the electrons at each moment in time, since the vibrational levels can store energy and redistribute it back later. However, integrated over the whole simulation time, the total vibrational energy loss is of course equal to the total vibrational energy received from the electrons.

The time dependent CO_2 conversion is again plotted against the right y-axis. The results are now shown for two different gas temperatures and only one value of E/N, since the vibrational energy pathways depend mostly on gas temperature and gas chemical composition. The E/N and ionization degree have thus only an indirect effect.

Note that the residence time can be deduced from Eq. (5) by replacing the SEI by 2 eV/molec. Given that the product "$N\mu_e$" is calculated from the EEDF and is almost constant for a given E/N, the residence time is almost proportional to gas temperature.

At $T_g = 300$ K, CO_2 dissociation upon impact with any neutral molecule M (i.e. reaction N1), is the main vibrational energy loss process, especially at the beginning of the plasma, accounting for up to 75% of the vibrational energy losses. The delay time between the start of the plasma and the effective start of dissociation processes is due to the time required for a significant vibrational population to build up. The second energy loss process is dissociation upon impact with O atoms in the plasma (i.e. reaction N2). At the beginning of the plasma, however, the contribution of N2 is negligible. This is because first O atoms need to be formed by reaction N1 or electron impact dissociation. At the end of the plasma, the vibrational energy dissipated by reaction N2 reaches 35% of the total vibrational energy losses.

VV energy exchanges between CO_2 molecules (i.e. reactions V5 and V6 in Table A.5 in Appendix A) are also non-negligible energy loss mechanisms. While the reaction rates of VV reactions between CO_2 molecules can be extremely high, the energy lost in each reaction is rather small. The energy loss in VV reactions is due to the anharmonicity between the energies of the vibrational levels. Because of the small energy losses, VV reactions only account for between 10% and 15% of the vibrational energy losses, in spite of their high reaction rates.

In a similar fashion, VV energy exchange between CO_2 and CO molecules (i.e. reaction V8 in Table A.5 in Appendix A) is non-negligible, and becomes increasingly important with time, due to CO_2 conversion into CO, hence giving rise to a higher CO density. As mentioned earlier, this process can create a large population of CO vibrationally excited states. It is thus important to consider the CO vibrational kinetics in this type of modeling, as also pointed out by Pietanza et al. [34].

Pure VT transfers (reactions V1, V2a, V2b and V2c in Table A.5 in Appendix A) cause only a small vibrational energy loss, due to the relatively low gas temperature considered here (300 K). Finally, since CO_2 electron impact dissociation occurs mainly from ground state CO_2 (as explained below) and is not a process likely to happen at low E/N, it is only a minor vibrational energy loss process here.

At $T_g = 1000$ K, the situation is very different, because VT energy transfer processes account for almost all the vibrational energy loss. Indeed, the rate coefficient of VT reactions (reactions V1, V2a, V2b and V2c in Table A.5 in Appendix A) increases rapidly with gas temperature. VV exchanges between CO_2 molecules are only a minor process, and the other processes are completely negligible. Indeed, as also pointed out in our previous work [22,26], with increasing gas temperatures, VT transfers become so important that vibration-induced dissociation becomes of minor importance.

To conclude this section, we have investigated the time-dependent behavior of the electron and vibrational energy loss pathways. We showed that at low E/N (50 Td), most of the electron energy effectively goes to CO_2 vibrational excitation, while at a higher E/N (150 Td), more energy-demanding processes such as electronic excitation and electron impact dissociation become important energy loss pathways as well. The vibrational energy is subsequently mostly lost to dissociative processes at low gas temperature (300 K), while at higher gas temperature (1000 K), VT vibrational energy loss processes become more important and dissipate the vibrational energy much faster.

As discussed below in more detail, the different energy transfers taking place in the plasma can explain the trends observed in Fig. 1. Indeed, we see that a high temperature quickly dissipates the vibrational energy, rendering vibration-induced dissociation unlikely. On the other hand, a low E/N value favors vibrational excitation, and thus also vibration-induced dissociation (at least at low gas temperature).

3.1.3. Time-integrated behavior of the energy transfers in the plasma

Figs. 2 and 3 present the time-dependent behavior of the different energy transfers for a few representative conditions. In order to compare the results in a wider range of conditions, we have integrated the energy losses over time in the plasma.

Fig. 4 shows the averaged electron temperature as a function of E/N in the plasma, calculated with Bolsig+, for different conditions of gas

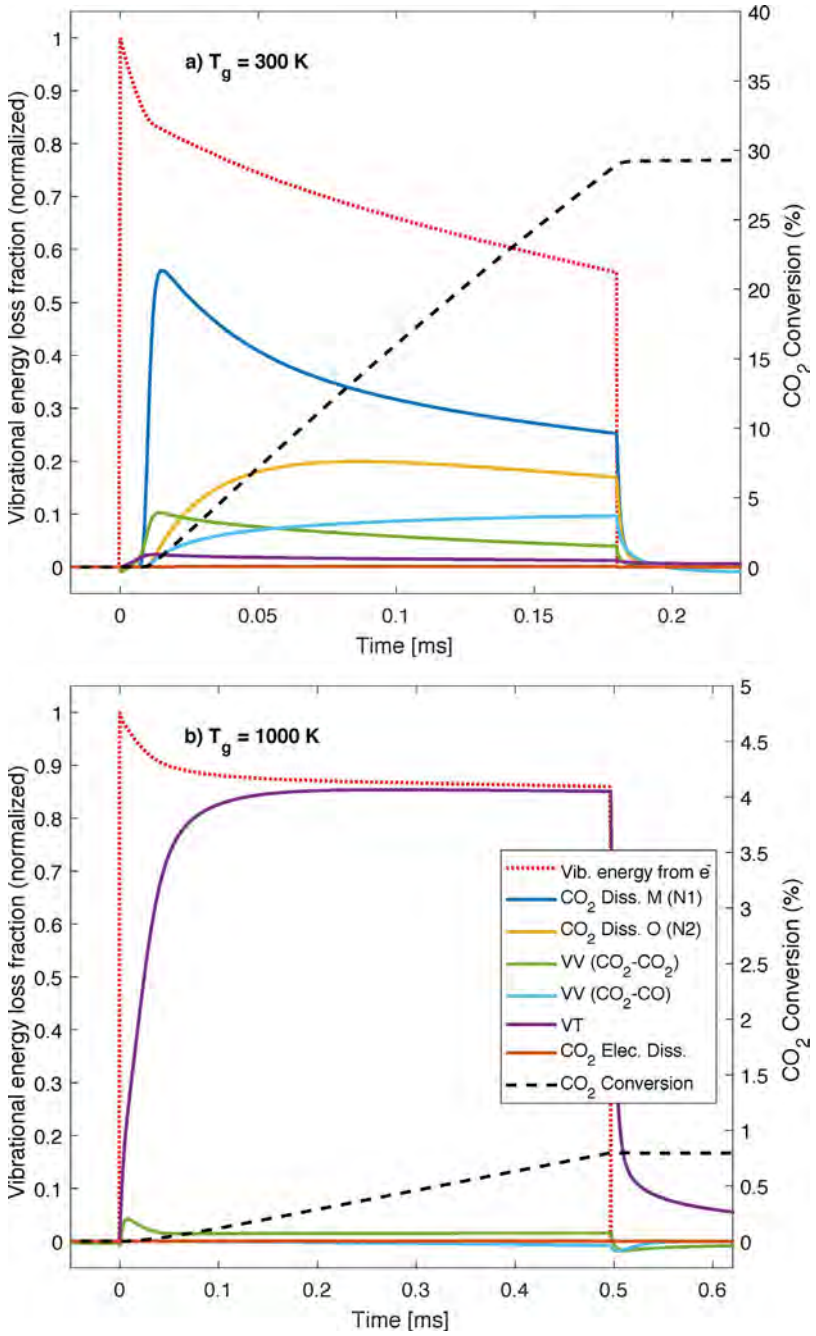

Fig. 3. Vibrational energy loss processes (left *y*-axis) and CO_2 conversion (right *y*-axis) as a function of time for a reduced electric field of 50 Td, an ionization degree of 10^{-6}, a pressure of 100 mbar and a gas temperature of 300 K (panel a, top) and 1000 K (panel b, bottom). The energy loss is normalized to the maximum of the total energy that the CO_2 vibrational levels received from the electrons.

temperature, and an ionization degree $\alpha_i = 10^{-6}$. This gives important information to understand better the role of *E/N*. Indeed, as expected, the electron temperature increases almost linearly with *E/N*: from 0.2 eV at 10 Td for T_g = 300 K, to 3.4 eV at 200 Td. A small difference can be seen for different gas temperatures. Indeed, the gas temperature can have a small effect on the electron kinetics, mostly indirectly by changing the gas composition, and thus affecting the energy losses by electron collisions with different plasma species, which will slightly influence the electron energy.

Fig. 5 shows the relative contributions of the time-integrated electron energy losses of the six main energy loss processes as a function of *E/N* and for a gas temperature of 300 K and an ionization degree of 10^{-6}.

Other minor processes accounting for the remaining electron energy losses (attachment reactions, CO ionization, etc.) are not shown here, for the sake of clarity. As there is no clear dependence to gas temperature in the electron energy pathways, the results of Fig. 5 can be considered representative of the different gas temperatures. Indeed, the electron energy pathways depend only on gas composition and EEDF. These two variables, and especially the gas composition, can be slightly affected by the gas temperature, as the latter slightly influences the CO_2 conversion and thus the CO_2 and CO density in the plasma, but the trends observed in Fig. 5 remain very similar for all the gas temperatures studied here.

At low *E/N*, CO_2 vibrational excitation is, by far, the main electron energy loss process. CO_2 vibrations receive up to 95% of the electron energy. The rest of the electron energy is lost to CO vibrations. Electron impact CO_2 dissociation starts to become non-negligible from 40 Td and

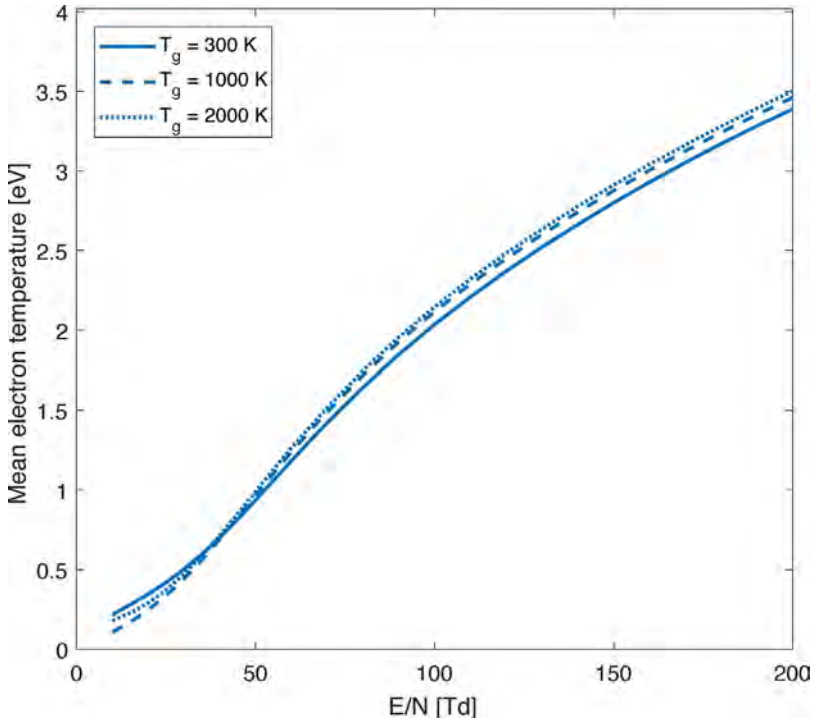

Fig. 4. Mean electron temperature averaged over the plasma for an ionization degree $\alpha_i = 10^{-6}$ and three different gas temperature (300 K, 1000 K and 2000 K).

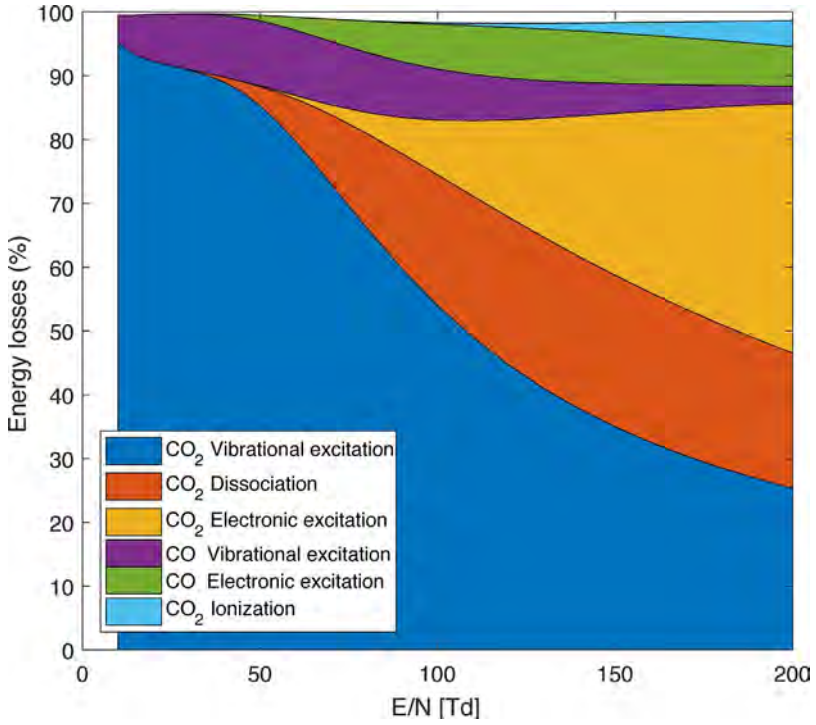

Fig. 5. Relative contribution of the main processes responsible for the electron energy loss as a function of the reduced electric field *E/N*, for a gas temperature of 300 K, an ionization degree of 10^{-6} and a pressure of 100 mbar. The electron energy losses are integrated over the plasma for each value of *E/N*.

accounts for up to 21% of the electron energy losses at high *E/N* (i.e. above 100 Td). CO_2 electronic excitation becomes more important around 60 Td and even becomes the main electron energy loss at high *E/N*, accounting for up to 39% of the electron energy losses at 200 Td.

The electron energy lost to CO varies between 4% and 13%. It is interesting to note that although the CO_2 conversion, and thus the CO density, decreases with increasing *E/N* (see Fig. 1)), the losses to CO are more important above 100 Td than at 45 Td. This can be explained by the relatively low energy threshold of CO electronic excitation (from 6.22 eV to 10.01 eV, see Table 1), which makes CO electronic excitation an important electron energy loss at high *E/N*.

The electron energy loss pathways depend only on the value of the reduced electric field and the density of the various species colliding with the electrons. Therefore, the results of Fig. 5 can be considered representative of all the conditions considered in this paper. At different gas temperatures and different ionization degrees, only the losses to CO

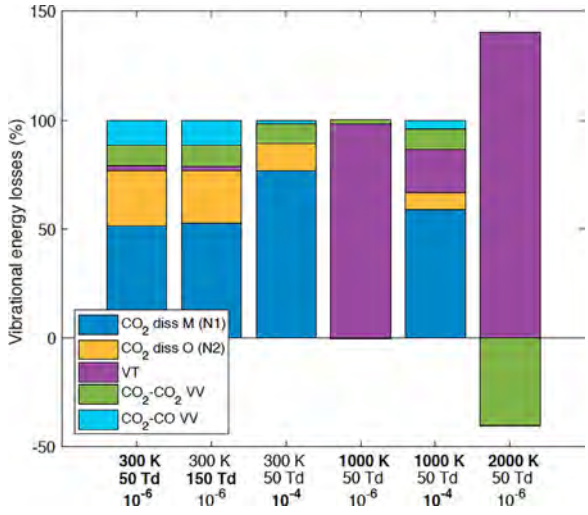

Fig. 6. Relative contribution of the main processes responsible for the vibrational energy losses integrated over time, for different conditions of gas temperature, reduced electric field and ionization degree, and at a pressure of 100 mbar. The parameters written in bold indicate the differences with the first case.

will vary to some extent, due to the change in CO density.

Fig. 6 illustrates the main processes responsible for the vibrational energy losses, for different conditions, integrated over time. The integrated energy losses are again normalized to the energy received by the CO_2 vibrational levels from the electrons.

As mentioned earlier, the value of E/N and the ionization degree only have an indirect effect on the vibrational energy pathways. However, some differences can still be found.

In the first, called 'standard' case, at $T_g = 300$ K, $E/N = 50$ Td and $\alpha_i = 10^{-6}$, as observed in Fig. 3a, the main vibrational energy loss process is reaction N1, i.e. dissociation of the vibrational levels upon collision with any molecule M (51%), followed by reaction N2, i.e. dissociation upon collision with an O atom (25%). CO_2–CO and CO_2–CO_2 VV reactions have a similar relative weight (each around 11%). VT relaxation only accounts for 2.5%. With a higher E/N (e.g. 150 Td), the results are practically identical; see second case.

Upon higher ionization degree, the plasma residence time to reach the same total SEI of 2 eV/molec (cf. Section 2.3) is much smaller (about a factor 100 for $\alpha_i = 10^{-4}$). Hence, there is less time for VT reactions to occur and the vibrational population becomes much larger.

Therefore, VT energy losses become negligible (in the entire range of E/N investigated), and dissociation upon impact with any molecule M is the main vibrational energy loss (76% at $\alpha_i = 10^{-4}$, 300 K and $E/N = 50$ Td see third case). As a consequence, the CO_2 conversion is somewhat higher (see Fig. 1).

Note that, at lower E/N, the energy deposition per time is smaller and thus the plasma residence time to reach 2eV/molec is longer. Therefore, at still lower E/N than 50 Td, VT relaxation as well as CO_2–CO VV relaxation still can become somewhat more important than in the cases shown here (i.e. 50 Td) and dissipate a larger proportion of the energy. In this case, the residence time is thus an important parameter in the dissipation of the vibrational energy, so if the residence time is 100-fold shorter at a 100 times higher ionization degree ($\alpha_i = 10^{-4}$ vs $\alpha_i = 10^{-6}$), VT and CO_2–CO VV relaxation again become negligible. This explains the higher conversion at very low E/N, observed in Fig. 1 upon higher ionization degree, and it also explains why the difference is larger than at 50 Td.

At $T_g = 1000$ K and $\alpha_i = 10^{-6}$ (case 4), almost all the vibrational energy is lost to VT relaxation and thus, there is very little vibration-induced dissociation. The very limited CO_2 conversion that occurs at this temperature (ca. 0.7%, see Fig. 1) is almost entirely due to electron impact processes, mainly electron impact dissociation.

On the other hand, with $\alpha_i = 10^{-4}$, the power density is much higher and thus the plasma residence time to reach the same SEI of 2 eV/molec is lower. This favors vibration-induced dissociation above VT relaxation (see case 5 in Fig. 6), although it needs to be mentioned that the O atoms do not recombine much with CO_2 molecules, as they do not have enough time, after creation, to collide with another CO_2 molecule within this short time. Nevertheless, because vibration-induced dissociation upon collision with any molecule M is again much more important at higher ionization degree, the CO_2 conversion is much higher (ca. 16%, see Fig. 1).

Finally, at $T_g = 2000$ K, CO_2–CO_2 VV reverse reactions become more important than the forward reactions, meaning that the highly energetic vibrational levels tend to be 'pumped down' towards the ground state; see last case in Fig. 6. VT transfers dissipate all the energy obtained by the vibrational levels, explaining why the CO_2 conversion is nearly negligible in Fig. 1.

Figs. 5 and 6 give clues to understand the trends observed in Fig. 1, namely the increase of CO_2 conversion and energy efficiency with decreasing reduced electric field, increasing ionization degree and decreasing gas temperature (in the range 300–2000 K).

To summarize, at lower E/N, the electrons transfer more of their energy to the vibrational modes of CO_2, while at higher E/N, electron impact dissociation and electronic excitation processes become prominent. These processes are costly, due to their high energy thresholds, and are thus detrimental to the energy efficiency. Because vibration-induced dissociation is the most efficient dissociation pathway, enhancing vibrational excitation leads to a better energy efficiency.

Furthermore, a higher gas temperature will lead to more VT energy losses, which renders vibration-induced dissociation very unlikely at temperatures of 2000 K (and above). A higher ionization degree originates from a higher power density, which in turn decreases the plasma residence time, for a given SEI. Decreasing the plasma residence time diminishes the VT energy losses and thus favors vibration-induced dissociation.

Experimentally, MW and GA plasmas, as well as glow discharges, work at moderate E/N values (around 50–100 Td). However, the ionization degree is typically rather low in these discharges (around 10^{-6}), notably due to the lower ionization rate coefficient at low E/N (i.e. lower electron temperature). Furthermore, the gas temperature can also be relatively high in these discharges [26], especially when they operate at relatively high pressure.

DBDs, on the other hand, operate at higher E/N (200 Td and above), which makes electron impact dissociation the main dissociative process. The vibrational population is thus not so important, and therefore, the fact that they exhibit relatively low gas temperatures and high ionization degrees does not lead to an improved conversion.

Hence, there is clearly room for optimization of the most common discharges used for CO_2 conversion, by using setups working simultaneously at low E/N, gas temperatures close to room temperature and high ionization degrees.

3.1.4. Vibrational distribution functions

The vibrational energy loss mechanisms are of course very dependent on the degree of vibrational excitation. Therefore, the shape of the VDF is an important parameter to understand the results of Fig. 6. Fig. 7 presents the VDFs in the middle of the plasma (i.e. half of the plasma residence time) for the same conditions as Fig. 6. The vibrational temperatures, indicated in Fig. 7, are calculated using the ratio of the populations of the first asymmetric mode vibrational state and the ground vibrational state. The equilibrium Boltzmann distributions corresponding to the same gas temperatures are shown with dashed lines. The shape of the VDF is determined by the relative importance of the different processes studied above, mainly electron impact vibrational excitation, VV and VT transfers, and dissociation reactions. The first part of the VDF can usually be described by a Treanor distribution [63], while the tail of the distribution is mostly influenced by

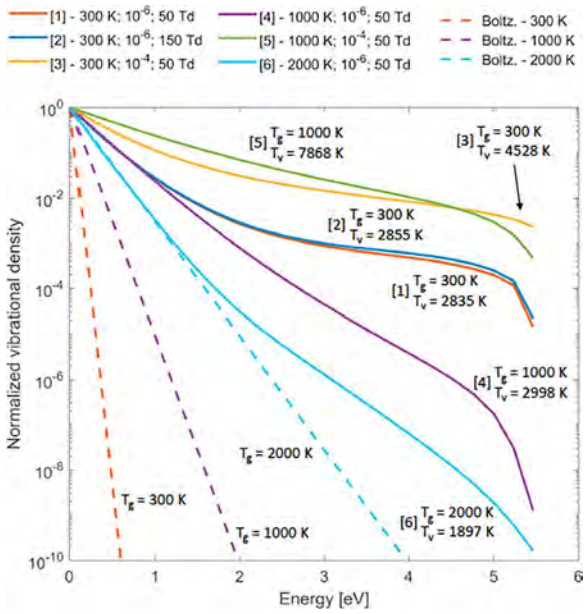

Fig. 7. Vibrational distribution functions (VDFs) of the asymmetric mode vibrational levels of CO_2 at half of the 'plasma residence time', for various conditions, as also presented in Fig. 6. The legend of each curve indicates the gas temperature, the ionization degree and the reduced electric field, respectively, and the numbers of the curves correspond to the cases of Fig. 6. Both the gas and vibrational temperature are indicated next to each number. The Boltzmann distributions corresponding to the gas temperatures considered here are shown with dashed lines.

dissociative processes, which are not included in Treanor's theory (see our previous work [26] for a more detailed comparison/discussion and the work of Diomede et al. [64]).

As also pointed out in our previous work [26], a higher gas temperature brings the VDF closer to thermal equilibrium (i.e. higher vibrational levels less overpopulated), by enhancing VT reactions (cf. cases 4 and 6 in Figs. 6 and 7, compared to the 'standard' case 1). The energy of the electrons is thus ultimately dissipated to heat and there is almost no vibration-induced dissociation.

This also explains the trends observed in Fig. 1. It is quite obvious that a large vibrational population is required in order to favor vibration-induced dissociation. Therefore, any condition favoring vibrational excitation will also favor vibration-induced dissociation, provided that VT energy losses are not too fast, thus provided that VT losses do not counter-balance the gain of a large vibrational excitation.

On the other hand, a higher ionization degree originates from a higher power density, which increases the electron impact vibrational excitation rate. This results in a VDF with a clear over-population of the higher vibrational levels compared to the Boltzmann case (see curves 3 and 5). This is even true at 1000 K (curve 5): although VT relaxation increases with temperature, a strong-enough electron impact vibrational excitation is still able to overcome this VT relaxation.

Finally, it is interesting to note that the two VDFs at $T_g = 300$ K and $\alpha_i = 10^{-6}$ with $E/N = 50$ Td and 150 Td practically overlap (i.e. curves 1 and 2). Indeed, although at higher E/N a smaller part of the electron energy goes to vibrational energy, it also gives a higher power deposition density. These two effects compensate each other here and make the two VDFs look very much alike. However, the residence time decreases with increasing E/N (or equivalently power density), so the total energy going to the vibrational levels (integrated over the whole simulation time) is still lower with a higher E/N.

3.1.5. Dissociation mechanisms

We now combine the above results of the electron energy transfers and vibrational energy transfers to elucidate the main processes responsible for CO_2 conversion. Their relative contributions are plotted in

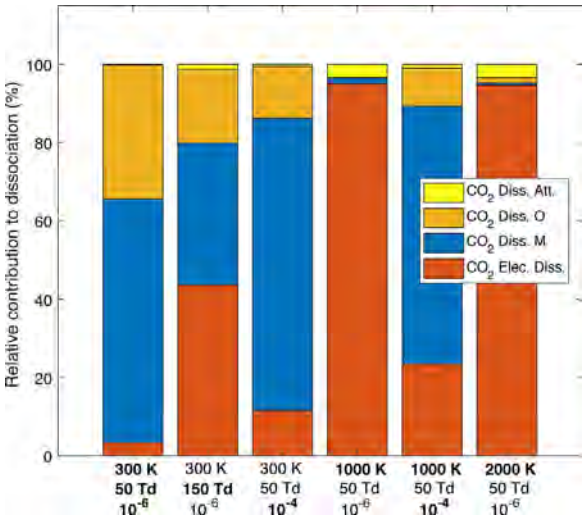

Fig. 8. Relative contribution of the main processes responsible for CO_2 dissociation for different conditions (as in Fig. 6), integrated over time, and at a pressure of 100 mbar. The parameters written in bold indicate the differences with the first case. The dotted and dashed lines show the activation energy of reactions (N1) and (N2), i.e. dissociation upon impact by any molecule M and upon O atom impact, respectively.

Fig. 8 for the same conditions as in Fig. 6. In the 'standard' case, the conversion is mainly caused by neutral dissociative reactions. The dissociation upon collision with any molecule M (N1, see Table A.4 in Appendix A) is responsible for about 62%, while the dissociation upon collision by an O atom (N2, see Table A.4 in Appendix A) accounts for 34%. Electron impact dissociation (X4, see Table A.1 in Appendix A) accounts for only 3% of the conversion.

Upon increase of the reduced electric field to 150 Td (case 2), the contribution of electron impact dissociation becomes much more important (44%), as can also be deduced from Fig. 2b. On the other hand, with $E/N = 50$ Td and $\alpha_i = 10^{-4}$ (case 3), the contribution of reaction N1 becomes much larger (75%). Indeed, the plasma residence time (to reach the same SEI of 2 eV/molec) is here much lower, so the O atoms created in reaction N1 do not have enough time to dissociate an extra CO_2 molecule.

At 1000 K, 50 Td and $\alpha_i = 10^{-6}$ (case 4), there is very little vibrational excitation (see Fig. 7). Therefore, the main mechanism is electron impact dissociation. Note that, although its relative contribution is close to 100% (Fig. 8), its absolute contribution is small, due to the low rate of this process, explaining the low CO_2 conversion in this case (cf. Fig. 1).

On the other hand, at 1000 K, 50 Td but $\alpha_i = 10^{-4}$ (case 5), the major processes resemble more the corresponding 300 K case (case 3), because there is now enough electron impact vibrational excitation due to the higher ionization degree. Still, the CO_2 conversion is lower than at 300 K (cf. Fig. 1), because of more prominent vibrational loss due to VT relaxation (cf. Fig. 6: case 5 vs case 3).

Finally, at 2000 K and $\alpha_i = 10^{-6}$ (case 6), only electron impact dissociation is possible, due to the strong VT relaxation, yielding only a very low population of the vibrational levels (cf. Fig. 7), just like in case 4. Again, although the relative contribution of electron impact dissociation is close to 100%, its absolute contribution is low, explaining the very low CO_2 conversion (see Fig. 1).

3.1.6. Vibrational energy consumption

When inspecting Figs. 8 and 6, a question raises itself. Why does dissociation reaction N2 (i.e. upon collision with O atoms) consume such a large proportion of the vibrational energy, despite its lower activation energy (E_a(N1) = 4.53 eV for N1 and E_a(N2) = 2.28 eV for N2) and lower reaction enthalpy than reaction N1 ($\Delta H°$(N1) = 5.52 eV for N1 and $\Delta H°$(N2) = 0.35 eV for N2)?

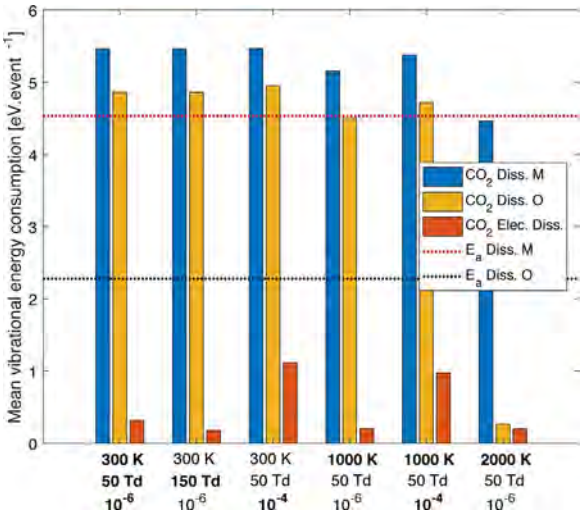

Fig. 9. Mean vibrational energy consumption per dissociation event for different conditions (as in Fig. 6), integrated over time, and at a pressure of 100 mbar. The parameters written in bold indicate the differences with the first case. The dotted lines show the activation energy of reactions (N1) and (N2), i.e. dissociation upon impact by any molecule M and upon O atom impact, in red and in black, respectively. (For interpretation of the references to color in this figure legend, the reader is referred to the web version of this article.)

Therefore, we plot in Fig. 9 the mean vibrational energy consumption per dissociation event, for the same conditions as in Figs. 6 and 8. The mean vibrational energy consumed by dissociation reaction l is calculated using:

$$E_{\mathrm{cons},l} = \frac{\sum_k R_{l,k} E_{\mathrm{vib},k}}{\sum_k R_{l,k}} \tag{8}$$

where the index k refers to each of the CO_2 vibrational levels, $E_{vib,k}$ is their energy, and $R_{l,k}$ is the reaction rate of the dissociation reaction l from this vibrational level k.

As explained in Section 2.2, in the absence of significant thermal excitation, only molecules with a vibrational energy $E_v \gtrsim E_a/\alpha$ can react in a reaction with activation energy E_a. E_a/α can thus be considered as an effective activation energy for vibration-induced dissociation reactions.

The vibrational energy of the reacting molecule is consumed in the reaction and the excess energy, i.e. $E_v - \Delta H°$, is wasted to heat. The mean vibrational energy consumption of a dissociation reaction is thus equal to the mean energy of the vibrational levels contributing to that reaction. For the most energy efficient dissociation processes, the mean vibrational energy consumption should be equal to the enthalpy of the dissociation reaction. The more the mean vibrational energy consumption exceeds above the enthalpy of that reaction, the more vibrational energy will be wasted (i.e. spent without strictly being needed for dissociation).

As the gas temperature increases, the molecules acquire translational energy, which they can also use to overcome the activation energy E_a of the reaction. Therefore, the mean vibrational energy can be less than the activation energy of the dissociation reaction. At high enough gas temperatures, molecules at the tail of the translation energy distribution can have enough translational energy to overcome the activation energy barrier without the help of vibrational excitation. The dissociation process is then more thermal than vibration-induced.

For all conditions shown in Fig. 9 here, the vibrational energy consumption of dissociation upon reaction N1 (i.e. collision with any molecule M) is close to its activation energy. More precisely, for temperatures of 1000 K and below, it is slightly higher, so it means that only the high vibrational levels can effectively dissociate through N1 and their vibrational energy is consumed in reaction N1.

However, CO_2 molecules reacting with O atoms (in N2) have on average (i.e. averaged over all vibrational levels) about twice the energy required to overcome the activation energy barrier, and thus also much more than the reaction enthalpy, so it means that this excess vibrational energy is wasted. The α_O parameter, chosen according to the Fridman–Macheret theory [5] ($\alpha_O = 0.5$), describes the efficiency of vibrational excitation to overcome the activation energy barrier. In pure vibration-induced dissociation, vibrational levels actually 'see' an activation energy of $E_a(\mathrm{N2})/\alpha_O$ for reaction N2, explaining why they need so much vibrational energy to react.

At 2000 K (case 6), the energy required to overcome the activation energy of N1 slightly decreases, due to thermal energy. The temperature is thus still not high enough to overcome the high activation energy of this reaction (4.52 eV) without the help of vibrational energy. The drop in vibrational energy consumption of N2 is, however, much more substantial for two reasons: (i) as seen in Fig. 7, there are less highly excited vibrational levels at $T_g = 2000$ K and (ii) the activation energy of N2 (2.28 eV) is lower than the activation energy of N1. The energy required to overcome the activation energy barrier of N2 can thus be given by the translational energy of the reacting molecules, instead of vibrational energy. Thus, the vibrational energy is not used in reaction N2 at 2000 K, since this process is now thermally-induced, but thermal conversion is not efficient whatsoever.

Note that in this case, as seen in Fig. 8, both N1 and N2 are minor dissociation processes since the population of highly excited vibrational levels is too low to induce significant vibration-induced dissociation.

CO_2 electron impact dissociation only consumes little vibrational energy in most cases, as it occurs mainly from the ground state. Indeed, although the rate coefficient of electron impact dissociation increases upon higher vibrational levels, the lower population of these levels typically compensates for the increase. It is interesting to note that in the cases with higher vibrational excitation, like cases 3 and 5, electron impact dissociation appears to occur preferably from vibrational levels around 1 eV. This is due to the large population of vibrationally excited states. No vibrational energy can be considered wasted here, since the electron energy consumed in electron impact dissociation decreases anyway when it occurs from a vibrationally excited state of CO_2.

As explained above and in Section 2.2, in pure vibration-induced conversion (i.e. no significant thermal energy), a CO_2 molecule needs a vibrational energy $E_v \gtrsim E_a/\alpha$ to react in endothermic dissociation reactions, such as N1 and N2. From the point of view of energy conservation, the minimum energy consumption of a reaction in standard conditions should be its enthalpy $\Delta H°$. Thus, we have $E_a/\alpha \geq \Delta H°$. However, in particular for reaction N2, the difference is quite large, since $E_a(\mathrm{N2})/\alpha_O = 4.5$ eV and $\Delta H°(\mathrm{N2}) = 0.35$ eV. Therefore, as an example, if a CO_2 molecule with a vibrational energy $E_v \gtrsim E_a(\mathrm{N2})/\alpha_O$ reacts in N2, a total vibrational energy of $E_v - \Delta H°(\mathrm{N2})$ can be considered wasted, since it is transformed into heat, while a vibrational energy of only $\Delta H°(\mathrm{N2})$ is effectively used for dissociation.

The high mean vibrational energy consumption of dissociation upon collision with O atoms appears to be a strong limitation to the energy efficiency obtained in the model, as this excess energy (above the reaction enthalpy) is just wasted. Indeed, the maximum theoretical energy efficiency obtained in our current model, at the most ideal conditions for energy efficient CO_2 conversion, is only around 45% (see Fig. 1), while experiments have reported energy efficiencies up to 90% at ideal conditions (i.e. strong vibrational excitation and thermal non-equilibrium, due to reduced pressure and supersonic flow in MW discharges [6]). Although these results have not yet been reproduced since then, more recent MW experiments also reveal energy efficiencies of about 50% at reduced pressure and supersonic flow, or at reverse vortex flow [9], at probably not-yet-ideal conditions (smaller reactor, lower power deposition). Moreover, even at non-ideal conditions (e.g. MW or GA at atmospheric pressure, where the VDF is too close to thermal [26,27,38,39]), the measured energy efficiency is already around 30% [13,10]. Thus, we may wonder whether this waste of vibrational

energy, as predicted by the model, might be overestimated, thus leading to an underestimation of the predicted energy efficiency.

It must be stressed that this result depends on our assumption for the value of the α_O parameter, which is adopted from Fridman [5], but it is subject to uncertainty. In our previous work, we investigated the effect of uncertainties on the rate coefficients of various reactions [47], but we did not study the effect of the α parameters. Therefore, we will consider in the following two sections the effect of the two α parameters of reactions N1 and N2 (Section 3.2.1) and of the activation energy of reaction N2 (Section 3.2.2), in particular with respect to the obtained CO_2 conversion and energy efficiency, in order to elucidate how the variation of these parameters can yield higher predicted values for the conversion and energy efficiency.

3.2. Influence of the dissociation rate coefficients on CO_2 conversion and energy efficiency.

3.2.1. Role of α in the CO_2 dissociation reactions N1 and N2

In this section, we vary the values of the α parameters of N1 and N2, the two main neutral dissociation reactions. There is of course no possibility to vary these parameters experimentally. However, knowing their effect on the plasma variables can help to design experiments used to determine these coefficients, as for now, they are estimated based on simplified theories [5] and their values also depend on the activation energies, which are also subject to uncertainties. We name these parameters α_M and α_O, for reaction N1 and N2, respectively.

Fig. 10 illustrates the behavior of the CO_2 conversion (left z-axis) and energy efficiency (right z-axis) as a function of α_M and α_O, at a gas temperature of 300 K, an ionization degree of 10^{-5} and a reduced electric field of 50 Td (Fig. 10a) and 150 Td (Fig. 10b). Note that the standard values of α_M and α_O, used up to now in the model, are 0.82 and 0.5, respectively (see cross symbols in Fig. 10).

At E/N = 50 Td, there is a sharp increase in the predicted CO_2 conversion and energy efficiency for $\alpha_M > 0.8$, reaching up to a maximum of 43% and 62%, respectively, for $\alpha_M = \alpha_O = 1$. The effect of α_O is much smoother than the effect of α_M. At the other end of the parameter space, $\alpha_M = \alpha_O = 0.25$ gives 7% conversion and 10% energy efficiency.

Conversely, at E/N = 150 Td, the effect of α_M and α_O is less pronounced. The CO_2 conversion and energy efficiency rise from 9% and 13%, respectively, for $\alpha_M = \alpha_O = 0.25$, to 22% and 32%, respectively, for $\alpha_M = \alpha_O = 1$. Since the role of electron impact dissociation is more important at 150 Td (cf. Fig. 8 above), it is indeed quite straightforward that the CO_2 conversion and energy efficiency would be less affected by the choice of the two α parameters.

In order to understand these variations of the CO_2 conversion and energy efficiency with the values of α_M and α_O, Fig. 11a shows the main processes responsible for CO_2 conversion and Fig. 11b depicts the mean vibrational energy consumption per dissociation event, for various values of the α parameters. The meaning of mean vibrational energy consumption per dissociation event was explained in detail in Section 3.1.6.

As illustrated in Fig. 11a, with low values of α_M and α_O, the conversion is almost entirely due to electron impact dissociation, both at 50 Td and 150 Td, explaining (i) why variations in the value of these α parameters do not largely affect the calculated conversion and energy efficiency, and (ii) why the resulting conversion and energy efficiency are rather limited, because electron impact dissociation is a less efficient process than neutral dissociation from the CO_2 vibrational levels (N1 and N2). With higher values of α_M and α_O, at 50 Td, the contributions of N1 and N2 are equally important, contributing for nearly 50%, while electron impact dissociation is only a minor process. On the other hand, at E/N = 150 Td, and $\alpha_M = \alpha_O = 1$, the three dissociation reactions have similar contributions to the overall CO_2 conversion.

Fig. 11b indicates that mean the vibrational energy consumption of N1 is close to the reaction enthalpy (5.52 eV) for $\alpha_M < 0.82$, both at 50 and 150 Td. This means that only the highest vibrational level of CO_2 reacts in reaction N1, i.e. the level with an energy almost equal to the enthalpy of reaction N1 (or, equivalently, to the dissociation energy of CO_2). On the other hand, with $\alpha_M = 1$, the mean vibrational energy consumption of reaction N1 becomes close to the activation energy (4.5 eV), again at both values of the reduced electric field. As E_a(N1) < $\Delta H°$(N1), this indicates that CO_2 molecules with vibrational energies significantly lower than the CO_2 dissociation energy can dissociate, in the absence of thermal energy, which should in theory not be possible. The fact that the model would allow that would mean that the energy is not conserved and thus we advise against the use of a value of α_M above 0.82 using this rate coefficient.

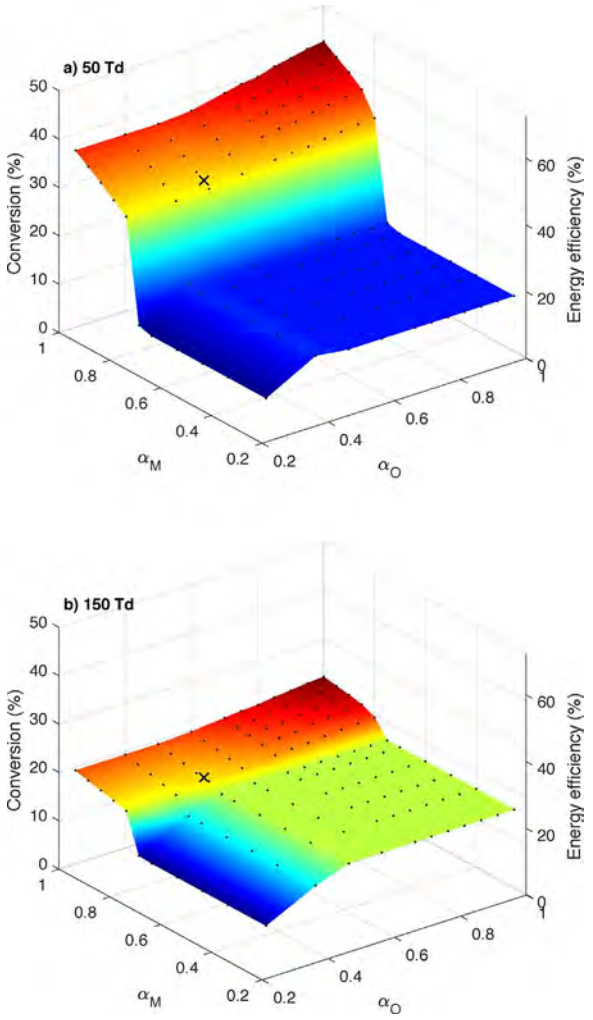

Fig. 10. CO_2 conversion and energy efficiency as a function of the α_M and α_O parameters, for a gas temperature of 300 K, an ionization degree of 10^{-5}, a pressure of 100 mbar, and a reduced electric field of 50 Td (panel a, top) and 150 Td (panel b, bottom). The cross symbols indicate the standard values of α_M and α_O, used up to now in the model, i.e. α_M = 0.82 and α_O = 0.5.

Baulch et al. pointed out in their review [65] that the activation energy of reaction N1 was significantly lower than the reaction enthalpy in the various experimentally derived values of the rate coefficient of reaction N1, but made no recommendation as to its value. They give two possible explanations for this anomaly: (i) the complexity of the reaction mechanisms of purely thermal CO_2 dissociation and (ii) the effect of impurities. More investigation will be needed to obtain a more accurate value of the rate coefficient, and in particular its activation energy, based on careful experiments in thermal conditions and on an improved analysis of the reaction scheme.

For reaction N2, on the other hand, the mean vibrational energy consumption decreases drastically with increasing values of α_O, both at 50 and 150 Td. With α_O = 1, the mean vibrational energy consumption

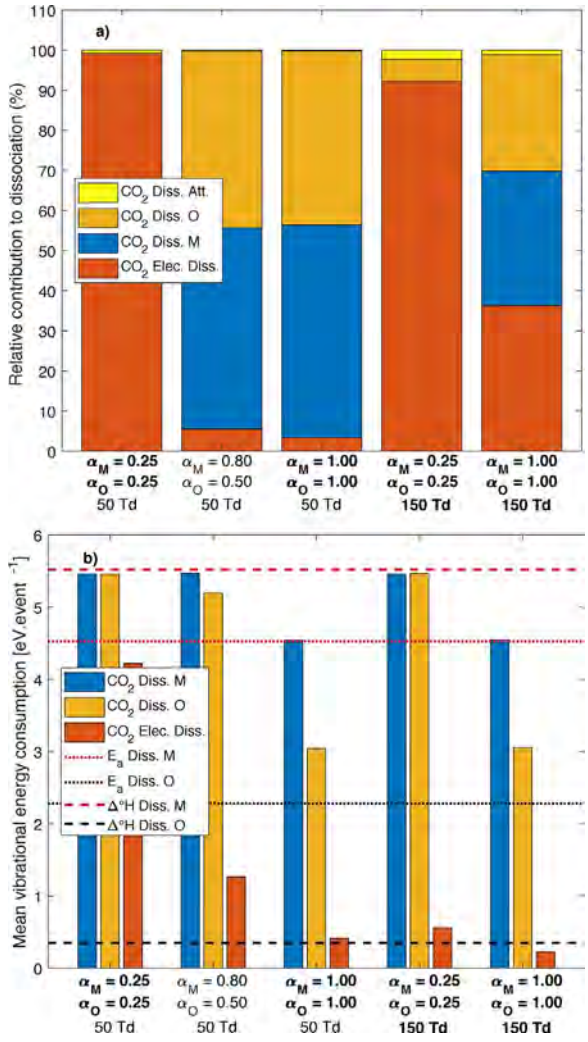

Fig. 11. Main processes responsible for CO_2 dissociation (a) and mean vibrational energy consumption per dissociation event (b) for different conditions, integrated over time, for a temperature of 300 K, an ionization degree of 10^{-5} and a pressure of 100 mbar. The parameters written in bold indicate the differences with the second case. The dotted and dashed lines in (b) show the activation energy and the standard reaction enthalpy, respectively, of reactions (N1) and (N2), i.e. dissociation upon impact by any molecule M and upon O atom impact, in red and in black, respectively. (For interpretation of the references to color in this figure legend, the reader is referred to the web version of this article.)

is close to the activation energy of the reaction (E_a(N2) = 2.28 eV), which means that the vibrational energy consumed by reaction N2 is only the energy necessary to overcome its activation energy. Reaction N2 then becomes much more likely to occur, which in turn increases the CO_2 conversion and the energy efficiency (cf Fig. 10). However, if reaction N2 becomes faster, the concentration of O atoms may become the limiting factor. That is why the contribution of dissociation by O atoms cannot exceed 50% of the total dissociation.

It may seem surprising that an increase of α_O does not lead to extra conversion for $\alpha_M < 0.7$. It can be explained as follows: reaction N1, for $\alpha_M \geq 0.8$, is efficient in dissociating the CO_2 molecules at the tail of the VDF and therefore depopulates it, resulting in the shape observed in Fig. 7. However, N1 is very unlikely to occur significantly for $\alpha_M < 0.7$. Therefore, the tail of the VDF becomes more and more populated and the distribution resembles the Treanor distribution [63] mentioned above. The population of the highly excited states then becomes even larger than that of the states with energies comparable to the activation energy of N2 (E_a(N2) = 2.28 eV). Hence, even at increased values of α_O, N2 is still more likely to take place from highly excited states, since they are more populated. However, due to the limiting concentration of O atoms, N2 is not efficient at depopulating the tail of the VDF, since it is not as fast as vibrational pumping. This results in a high mean vibrational energy consumption of N2, much higher than its activation energy, despite an α_O close to 1, and is responsible for the relatively low conversion and energy efficiency at high α_O and low α_M.

It is also interesting to note that for $\alpha_M = \alpha_O = 0.25$ and $E/N = 50$ Td, because neutral dissociation reactions are practically not occurring, the vibrational energy is partially dissipated by electron impact dissociation, while at higher values of the α parameters or higher E/N, the vibrational energy consumed by electron impact dissociation is nearly negligible.

Finally, the comparison of the case with $\alpha_M = 0.8$ and $\alpha_O = 0.5$ at $E/N = 50$ Td with case 1 of Fig. 8 (same conditions but with $\alpha_M = 0.82$) illustrates the competition between reactions N1 and N2. Indeed, shifting α_M only from 0.8 to 0.82 changes the ratio $\frac{R(N1)}{R(N2)}$ from 1.1 (Fig. 11b) to 1.77 (Fig. 9). That is because the pre-exponential factor of reaction N1 is higher than that of reaction N2 (see Table A.4 in Appendix A), and because the concentration of O atoms can limit reaction N2. However, both reactions require highly excited vibrational levels of CO_2 to overcome their activation energy barrier. Thus, enhancing reaction N1 is detrimental for reaction N2, because it will consume the highly excited vibrational levels of CO_2 that would have reacted in N2 otherwise.

This value of $\alpha_M \approx 0.82$ can be considered as a sort of critical value α_{crit} for reaction N1, which can be understood from the discussion related to Eqs. (1) and (2) (see Section 2.2). At low gas temperature (i.e. well below the activation energy), reaction N1 can only be significant if the vibrational energy of the CO_2 molecule (E_{vib}) follows $\alpha_M E_{vib} \gtrsim E_a$(N1). In our state-to-state model, the highest vibrational level considered is CO_2[v21], with a vibrational energy $E_{v21} = 5.47$ eV, i.e. close to the dissociation limit ($\Delta H°$(N1) = 5.52 eV). Therefore, for N1 to occur, it is required that $\alpha_M \gtrsim E_a/E_{v21} \simeq 0.83$, which explains the sharp rise in CO_2 conversion and energy efficiency for $\alpha_M > 0.8$, also noted in Fig. 10 a. Note that with $\alpha_M = 0.82$, as standardly used in our model, this reaction can still occur for the highest vibrational levels, as thermal energy still has a small contribution.

The fact that this ratio R(N1)/R(N2) is so sensitive to the change of α_M around 0.8 is due to the fact that $\alpha_M E_{v21} \approx 4.5$ eV = E_a(N1) for $\alpha_M \approx 0.82$, where E_{v21} is the energy of the highest CO_2 vibrational level. Therefore, for $\alpha_M < 0.8$, even the highest vibrational level CO_2[v21] sees an activation energy, while it only sees a small activation energy (or even none) for $\alpha_M > 0.8$.

To sum up the findings of this section, we first recommend to use a value of $\alpha_M = 0.82$, following the explanations given above. Using a higher value of α_M may lead to loss of energy conservation and is thus not recommended. The model results are less sensitive to the value of α_O and we can consider at this stage that a value of 0.5 gives reasonable results, i.e. following Eq. (2) with the rate coefficient presented in Table A.4 in Appendix A. Although the energy losses due to reaction N2 have been identified as being the limiting factor for energy efficient CO_2 conversion, an increase of the value of α_O does not lead to a very significant improvement of the energy efficiency calculated by the model, especially when using the recommended value of $\alpha_M = 0.82$. Therefore, the difference between the values of energy efficiency determined by the experiments and predicted by the model cannot be solely explained by the choice of α_O. However, as mentioned above, the activation energy of N2 is also subject to uncertainties. The effect of the activation energy of N2, and its coupling with the value of α_O, may thus provide better insights on the limitations to the energy efficiency predicted by the model.

3.2.2. Role of the activation energy of dissociation reaction N2

In our previous work on the uncertainties in the rate coefficients [47], we assumed that the uncertainty was contained in the pre-

exponential factor. This choice is valid in a given temperature range, where the rate coefficient has been derived experimentally and where the uncertainty in the pre-exponential factor also contains the uncertainty in the activation energy.

However, the uncertainty on the activation energy of the various reactions considered in this model can be particularly important when dealing with vibrationally excited molecules. Indeed, the previous assumption may not hold anymore, as the vibrationally excited levels will lower this activation energy, so the effect of uncertainty can become quite critical. The choice of the parameter α is closely related to the value of the activation energy considered. Given the variety of rate coefficients found for reaction N2 [48,65,5] and the differences in their activation energies, it is likely that the rate coefficient considered in our model overestimates its activation energy. Indeed, values ranging between 1.4 eV and 2.9 eV are found in the NIST database [48], while Baulch et al. [65] recommend a value of 2.28 eV (considered in our model) and Fridman [5] considers a value of 1.43 eV. Baulch et al. [65], being a review of various sources, appeared to us as the most reliable source.

Following the work of Kozak and Bogaerts [22], we study in this section the effect of the activation energy of N2 and its coupling with α_O. Note that we have kept the pre-exponential factor of the rate coefficient constant. This means that the rate coefficient of N2 increases exponentially with decreasing activation energy. Since ΔH°(N2) = 0.35 eV/molec is the theoretical minimum, we consider values of E_a(N2) from 0.35 eV to 2.5 eV. We consider here 2.5 eV as a maximum value of the activation efficiency, since 2.28 eV, the value adopted in our model, may already be an overestimation, given the fact that our predicted energy efficiency is limited compared to some experimental record values in literature.

We do not study here the effect of the value of the activation energy of reaction N1, since by our choice of $\alpha_M = 0.82$, we ensure that only CO_2 molecules with vibrational energies close to the dissociation limit can effectively dissociate through N1. Moreover, given that most experimentally derived value of E_a(N1) are even below the reaction enthalpy, as explained above, it seems unlikely that the activation energy of this reaction is significantly higher than the reaction enthalpy (5.52 eV).

Fig. 12 illustrates the CO_2 conversion (left z-axis) and energy efficiency (right z-axis) as a function of E_a(N2) and α_O, again at a gas temperature of 300 K, an ionization degree of 10^{-5} and a reduced electric field of 50 Td (Fig. 12a) and 150 Td (Fig. 12b). A value of 0.82 is considered for α_M, in accordance with the first section of our paper (Section 3.1) and with the recommendations of Section 3.2.1.

At 50 Td (Fig. 12a), the conversion and energy efficiency vary from 30% and 43%, respectively, for E_a(N2) = 2.5 eV and $\alpha_O = 0$, to 50% and 72%, respectively, with E_a(N2) = 0.35 eV and $\alpha_O = 1$. The increase is quite smooth with both α_O and E_a(N2), in comparison with the increase in CO_2 conversion caused by α_M (Fig. 10).

At 150 Td (Fig. 12b), the conversion and energy efficiency vary from 17% and 25%, respectively, for E_a(N2) = 2.5 eV and $\alpha_O = 0$, to 29% and 42%, respectively, with E_a(N2) = 0.35 eV and $\alpha_O = 1$. The evolution of the CO_2 conversion and energy efficiency with α_O and E_a(N2) resembles that of the 50 Td case, but with lower absolute values.

To understand these results, Fig. 13 again presents the relative importance of the main processes responsible for CO_2 conversion (Fig. 13a) and the mean vibrational energy consumption per dissociation event (Fig. 13b) for different choices of α_O, E_a(N2) and E/N. The results are integrated over time, for a temperature of 300 K, an ionization degree of 10^{-5} and a pressure of 100 mbar.

The reaction rate of N2 is subject to a very strong influence of both α_O and E_a(N2). In the most favorable case (i.e. E_a(N2) = 0.35 eV and $\alpha_O = 1$), reaction N2 accounts for half of the CO_2 conversion, both at 50 and 150 Td (see cases 3 and 5 in Fig. 13a). This means that all the O atoms produced by the other CO_2 dissociation reactions (i.e. upon collision with any molecule M, or due to electron impact dissociation,

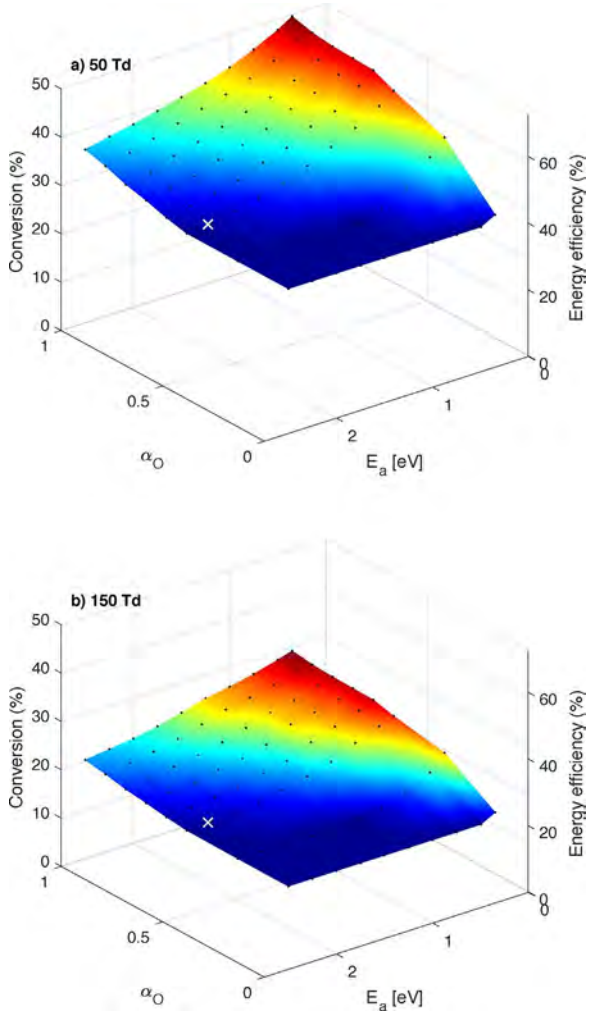

Fig. 12. CO_2 conversion and energy efficiency as a function of the α_O parameter and the activation energy of reaction N2, for a gas temperature of 300 K, an ionization degree of 10^{-5}, a pressure of 100 mbar, and a reduced electric field of 50 Td (panel a, top) and 150 Td (panel b, bottom). The cross symbols indicate the standard values of E_a(N2) and α_O, used up to now in the model, i.e. E_a(N2) = 2.28 eV and $\alpha_O = 0.5$.

which is important at 150 Td; cf Fig. 13a) dissociate an extra CO_2 molecule. The presence of O atoms is then the limiting factor for reaction N2 to occur. On the other hand, with a low value of α_O, the relative contribution of N2 to CO_2 conversion is practically negligible (cf. cases 1 and 4 in Fig. 13a, for $\alpha_O = 0.25$). This means that the O atoms produced by CO_2 conversion will recombine together, forming O_2, and thus will not contribute to the conversion of CO_2.

In case 2, reaction N2 still accounts for almost half of the total dissociation, despite an activation energy of 2.25 eV. That is due to the competition between reactions N1 and N2 to dissociate the highly excited vibrational levels of CO_2, as explained above in Section 3.2.1. With $\alpha_O = 1$ and E_a(N2) = 2.25 eV, reaction N2 can easily occur for vibrational energies above 2.25 eV, hence the second half of the VDF. N2 can thus occur with vibrational levels that cannot react with N1, and the concentration of O atoms becomes then again the limiting factor of N2. Hence, the mean vibrational energy consumption of N2 drops to about 3.2 eV, as can be observed in Fig. 13b.

As expected, the mean vibrational energy consumption of reaction N2 is strongly affected by both α_O and E_a(N2), as is clear from Fig. 13b. Increasing α_O and/or decreasing E_a(N2) allows the O atoms to react with lower vibrationally excited CO_2 molecules and still give rise to dissociation, thus reducing the mean vibrational energy consumption, and hence improving the conversion and energy efficiency predicted by

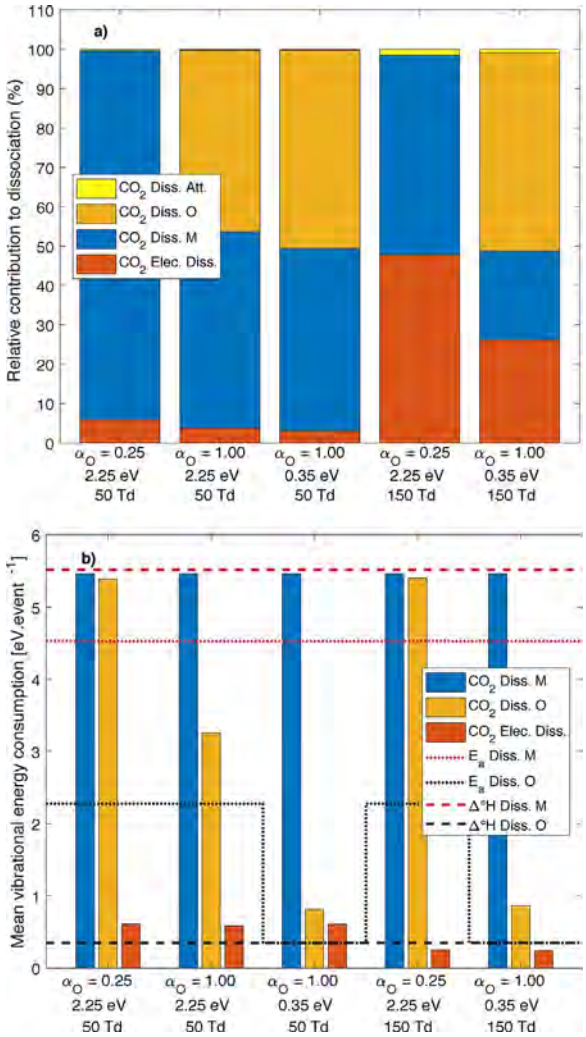

Fig. 13. Main processes responsible for CO_2 dissociation (a) and mean vibrational energy consumption per dissociation event (b) for different conditions, integrated over time, for a temperature of 300 K, an ionization degree of 10^{-5} and a pressure of 100 mbar. The dotted and dashed lines in (b) show the activation energy and the standard reaction enthalpy, respectively, of reactions (N1) and (N2), i.e. dissociation upon impact by any molecule M and upon O atom impact, in red and in black, respectively. Note that the activation energy of reaction N2 is not the same for the different cases, as indicated below the *x*-axis for each case. (For interpretation of the references to color in this figure legend, the reader is referred to the web version of this article.)

the model (cf Fig. 12).

3.3. Maximum theoretical energy efficiency

We have seen in the previous sections that the excess vibrational energy required to overcome the activation energy barrier of the two main dissociation reactions, i.e. N1 and N2, leads to a considerable energy loss for the conversion, especially concerning reaction N2. In this section, we derive a formula that gives the maximum energy efficiency that can be reached in the model. This formula is derived to give a mathematical framework to the observations of the previous sections. More specifically, it provides insight in the effect of the input parameters in the model (i.e. activation energies of reactions N1 and N2, and corresponding α parameters, being a measure for the efficiency of the vibrational levels to overcome these activation energies) for predicting the theoretical maximum energy efficiency. Furthermore, it is helpful in order to understand how the experimental energy efficiency can be improved. The actual values of the activation energy and α parameters are not used in this section on purpose, given the uncertainties present on their values.

In conditions of pure vibration-induced dissociation, the minimum vibrational energy required to dissociate a CO_2 molecule through either N1 or N2 is given by E_a/α. The products of the dissociation reactions (i.e. CO and/or O_2) are assumed to be formed in ground vibrational state. Thus an energy of at least $E_a/\alpha - \Delta H^\circ$ is dissipated into heating. For reaction N1, we have used $E_a(\mathrm{N1})/\alpha_M = 4.53\,\mathrm{eV}/0.82 = 5.52\,\mathrm{eV}$ as standard values in our model. In the case of reaction N2, we have considered $E_a(\mathrm{N2})/\alpha_O = 2.28\,\mathrm{eV}/0.5 = 4.56\,\mathrm{eV}$. Thus, in our standard model, only the vibrational levels with energy $\gtrsim$5.52 eV and 4.56 eV can contribute to CO_2 dissociation through N1 and N2, respectively, in the absence of thermal (translational) energy, i.e. in the case of pure vibration-induced dissociation. For N1, this means that only the highest vibrational level (v_{21}) can contribute, in the absence of thermal (translational) energy.

In the case of electron impact dissociation, an electron energy $E_{e^-,\mathrm{diss}}$ is consumed by each event, where $E_{e^-,\mathrm{diss}}$ is the energy threshold of electronic dissociation. In this study, we have considered $E_{e^-,\mathrm{diss}} = 7$ eV, as advised by previous research [41,42].

The following inequality is thus verified:

$$E_a(\mathrm{N2})/\alpha_O < E_a(\mathrm{N1})/\alpha_M < E_{e^-,\mathrm{diss}} \tag{9}$$

Note that since reaction N2 requires O atoms to be created by previous dissociation reactions in order to occur, we have $R_{\mathrm{N1}} + R_{e^-,\mathrm{diss}} \geq R_{\mathrm{N2}}$, where R_{N1}, R_{N2}, $R_{e^-,\mathrm{diss}}$ are the reaction rates of reaction N1, N2 and electron impact dissociation, respectively.

Given inequality (9), the best energy efficiency, or equivalently the lowest energy cost per CO_2 molecule converted, is reached for $R_{\mathrm{N1}} = R_{\mathrm{N2}}$ and $R_{e^-,\mathrm{diss}} = 0$. In other words, this means that CO_2 molecules are first dissociated by reaction N1 and the O atom produced subsequently reacts again in reaction N2 to dissociate another CO_2 molecule.

Following all these considerations, we can derive a formula of the minimum energy cost per CO_2 molecule converted:

$$E_{\mathrm{cost}} = \frac{1}{2}\{E_a(\mathrm{N1})/\alpha_M + E_a(\mathrm{N2})/\alpha_O\} \tag{10}$$

The $\frac{1}{2}$ factor originates from the fact that two CO_2 molecules are converted by reaction N1 followed by reaction N2. Note that this formula effectively gives the minimum energy cost, as it assumes that the total energy cost is only due to vibrational energy cost, i.e. considering pure vibration-induced dissociation, which is the most energy efficient dissociation process, as discussed above.

This yields a simple formula for the maximum energy efficiency, depending only on the activation energies of both neutral-induced dissociation reactions N1 and N2, and the corresponding α parameters (i.e. efficiency of the vibrational levels to overcome these activation energies):

$$\eta_{\mathrm{max}} = \frac{2.93\,\mathrm{eV/molec}}{\frac{1}{2}\{E_a(\mathrm{N1})/\alpha_M + E_a(\mathrm{N2})/\alpha_O\}} \tag{11}$$

As mentioned above, 2.93 eV/molec is the reaction enthalpy of $CO_2 \rightarrow CO + \frac{1}{2}\,O_2$.

It is useful to know that this formula is based on the following assumptions:

1. The conversion mechanisms are purely vibration-induced and not thermal. This means that the mean translational energy of the molecules is much lower than the activation energy of the different reactions. Following the results of Section 3.1, this approximation is not valid anymore at gas temperatures of 2000 K and above. However, thermal processes are typically less energy efficient than non-thermal processes [5]. The formula is thus likely to still be verified in the thermal case.
2. The excess vibrational energy needed by CO_2 molecules to overcome the activation energy barrier of a dissociative reaction is lost to heat.

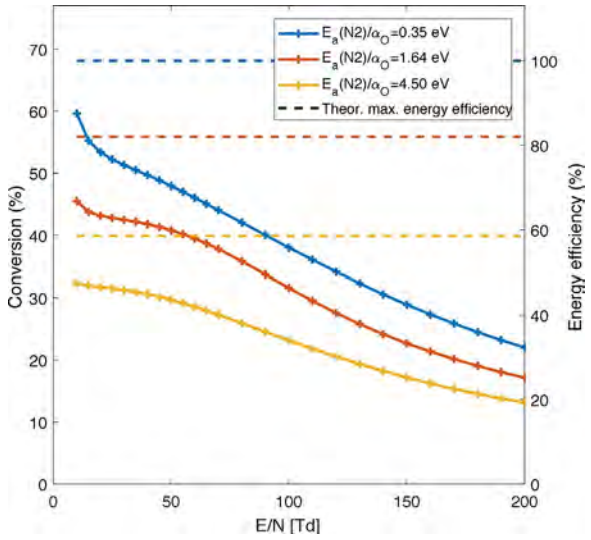

Fig. 14. CO_2 conversion (left *y*-axis) and corresponding energy efficiency (right *y*-axis) as a function of the reduced electric field *E/N*, for three values of $E_a(N2)/\alpha_O$ (0.35 eV, 1.64 eV, 4.50 eV), and for a gas temperature of 300 K, and an ionization degree of 10^{-4}. The dashed lines indicate the corresponding maximum theoretical energy efficiency using Eq. (11) in each case. The value of $E_a(N1)/\alpha_M$ is taken equal to 5.52 eV, as in our standard model.

This implies that the CO molecules created are in ground state. In reality, CO might however acquire part of the surplus vibrational energy after dissociation, which could actually increase the energy efficiency of the conversion. Indeed, given the fast VV CO_2–CO transfers, this CO vibrational energy could transfer to CO_2 vibrational modes and used again for dissociation, and thus it might not all be wasted.

Fig. 14 presents the CO_2 conversion (left *y*-axis) and corresponding energy efficiency (right *y*-axis), predicted by our model, as a function of the reduced electric field *E/N* for a gas temperature of 300 K and an ionization degree α_i of 10^{-4}, i.e. the conditions showing the maximum conversion and energy efficiency in Fig. 1, and for three different values of $E_a(N2)/\alpha_O$ (0.35 eV, 1.64 eV and 4.50 eV). A value $E_a(N1)/\alpha_M = \Delta H^\circ(N1) = 5.52$ eV is considered here, as in Section 3.1.

The last value corresponds to our standard model, with $E_a(N2)/\alpha_O = 2.28$ eV and $\alpha_O = 0.5$; the first value corresponds to the minimum $E_a(N2)$ of 0.35 eV (equal to the reaction enthalpy) and $\alpha_O = 1$ (see Section 3.2.2); and finally, the middle value is $E_a(N2)/\alpha_O = 1.64$ eV, with $E_a(N2) = 1$ eV and $\alpha_O = 0.61$, as calculated with the Fridman–Macheret model (Eq. (2)).

The dashed lines of the corresponding colors indicate the maximum theoretical energy efficiencies calculated with Eq. (11), for these three different values of $E_a(N2)/\alpha_O$, yielding 100%, 82% and 58%, respectively. These results are shown to see how this maximum theoretical energy efficiency, which is determined based on the rate coefficient expressions of N1 and N2 (more specifically the activation energies and corresponding α parameters), influences the results of CO_2 conversion and energy efficiency. Note that a value of $E_a(N2)/\alpha_O = 4.5$ eV corresponds to the case presented in Fig. 1 (standard model).

The increase in CO_2 conversion and energy efficiency upon lower *E/N*, that was observed in Fig. 1 (for $E_a(N2)/\alpha_O = 4.5$ eV) for low *E/N* becomes even more pronounced with lower values of $E_a(N2)/\alpha_O$, especially with 0.35 eV (i.e. $E_a(N2)/\alpha_O = \Delta H^\circ(N2)$). The maximum energy efficiency calculated at 10 Td is 46%, 65% and 86% for $E_a(N2)/\alpha_O = 4.5$ eV, 1.64 eV and 0.35 eV, respectively. In all three cases, the maximum energy efficiency calculated by the model (i.e. at 10 Td) is thus quite close to the theoretical maximum energy efficiency, derived following Eq. (11). This implies that the conditions plotted in Fig. 14, i.e. $T_g = 300$ K, $E/N = 10$ Td and $\alpha_i = 10^{-4}$, are quite optimal. The fact that the maximum calculated energy efficiency is not entirely equal to the theoretical maximum is due to other losses, that are not accounted for in the formula of Eq. (7), i.e. the fact that not all plasma power goes into electron energy, and especially that not all electron energy goes into vibrational excitation; see below.

At low pressure (1550 Pa), Andreev et al. [60] showed that their CO_2 glow discharge was self-sustained for reduced electric fields of 38.4 Td and above. In order to reach lower values of *E/N*, a second power source, enhancing ionization using a higher *E/N* had to be used. Therefore, these low values of *E/N*, especially 10 Td, in combination with an ionization degree of 10^{-4}, may be difficult to reach experimentally, unless a second power source is used. These values can however be considered as recommendations towards future experiments. Indeed, as also discussed in Section 3.1.3 above, there is clearly room for optimization of the most common discharges used for CO_2 conversion, by using setups working simultaneously at low *E/N*, gas temperatures close to room temperature and high ionization degrees.

Using particularly favorable conditions (10 Td, 300 K, $\alpha_i = 10^{-4}$), and $E_a(N1)/\alpha_M = \Delta H^\circ(N1)$ and $E_a(N2)/\alpha_O = \Delta H^\circ(N2)$, our model predicts a maximum energy efficiency of 86%. This value seems to be a practical limit for the energy efficiency due to the kinetics of the CO_2 discharge, and in particular the fact that electrons always lose part of their energy to processes other than CO_2 vibrational excitation (see Fig. 5). Indeed, the latter is not included in the formula for the maximum theoretical energy efficiency (Eq. (11)), yielding a value of 100% in this case. Using a lower SEI may reduce the electron energy losses to CO vibration and electronic excitation, since it would also reduce the conversion and thus the CO density.

The fact that the energy efficiency presented in Fig. 1 does not reach this maximum value of 86% is thus entirely due to the choice of the rate coefficient expressions (i.e. the value of the activation energies and α parameters). Using the values presented in Kozak and Bogaerts [22] and in Fridman [5], i.e. $E_a(N1) = 5.58$ eV, $E_a(N2) = 1.43$ eV, $\alpha_M = 1$ and $\alpha_O = 0.5$, we obtain a maximum energy efficiency of 70%. However, in our recent study on the uncertainties in the rate coefficients [47], we have not been able to verify the origin of these rate coefficients, and therefore we are reluctant to use them in our standard model. This greatly underlines the importance of the choice of rate coefficients and values of α.

To sum up, experimentally, energy efficiencies up to 90% have been reported [6] in non-thermal conditions. Assuming these are not the result of experimental errors, two explanations can be considered for the differences between the maximum model predictions and the maximum experimental CO_2 conversion and energy efficiency in conditions of pure vibration-induced dissociation.

(i) A first explanation could be due to uncertainties in the activation energy of the neutral dissociation reactions, as discussed in this paper. Assuming that $E_a(N1)/\alpha_M = 5.52$ eV, i.e. the enthalpy of the reaction, Eq. (11) yields that in order to have $\eta_{max} \gtrsim 90\%$, it is required to have $E_a(N2)/\alpha_O \lesssim 1$ eV. To our knowledge, there are no measurements of $E_a(N2)$ that would yield $E_a(N2)/\alpha_O \lesssim 1$ eV. Therefore, while it is possible that the conversion and energy efficiency are underestimated in our model due to the uncertainties in the rate coefficients, it is unlikely that an energy efficiency of 90% could be reached only by considering a more accurate value for $E_a(N2)/\alpha_O$.

(ii) Another explanation could be that the second assumption listed above is not fulfilled, i.e. the vibrational modes of the dissociation products, and in particular CO, receive part of the surplus vibrational energy in a dissociation event. This energy could then be redistributed to CO_2 vibrational modes and be used again for dissociation, thus increasing the energy efficiency of the conversion. To our knowledge, there is no study quantifying this phenomena, but we plan to investigate this in our future work.

Moreover, some other dissociation pathways might be important that are not yet included in the model due to lack of information on their kinetics. In particular, O atoms in electronic excited states are not

considered in this work and they could have an influence on the CO_2 dissociation mechanism.

The activation energy of the reaction of CO_2 dissociation upon collision with O atoms seems to be, in any case, a limiting factor to energy-efficient CO_2 conversion, as it is much higher than the reaction enthalpy. A way to enhance the energy efficiency could be the combination of plasma and catalysis. Indeed, a catalyst could enhance the dissociation rate of CO_2 upon collision with O atoms by lowering the activation energy barrier of this reaction, thus also reducing its vibrational energy consumption. Promising results have been obtained in the field of plasma-catalysis [66–68], although more research is needed to precisely understand the mechanisms of the plasma-catalyst interactions in plasma-catalytic CO_2 conversion.

4. Conclusion

We have elucidated the underlying (energy transfer) processes and the limiting reactions for energy efficient CO_2 conversion in a non-equilibrium plasma, in a range of different conditions, by means of a zero-dimensional chemical kinetics model.

In the first section, we show the electron energy losses and the vibrational energy losses, as well as the VDFs and the contributions of the various processes to CO_2 conversion, varying the reduced electric field, the ionization degree and the gas temperature, and we use these results to explain the calculated CO_2 conversion and energy efficiency in this range of conditions. In the second section, in order to understand the theoretical limitations to the energy efficiency, we vary the values of the α parameters for the neutral dissociation reactions and the activation energy of the dissociation of CO_2 upon impact with O atoms, and we investigate their effect on both the CO_2 conversion and the energy efficiency, as well as on the underlying dissociation mechanisms and their energy consumption.

The model reveals the important role of vibrational excitation, particularly at low gas temperatures. A lower E/N increases the contribution of the electron energy going to vibrational excitation of CO_2. Furthermore, at low gas temperatures, this leads to a large part of the energy used for dissociation, upon collision of the vibrational levels with neutral molecules (either molecules M or O atoms), which is thus beneficial for the energy efficiency. At higher gas temperatures, VT relaxation becomes more prominent, so the vibrational energy primarily dissipates to heat. The ionization degree also has an important effect, since a higher ionization degree leads to a shorter plasma residence time (to reach the same fixed specific energy input of 2 eV/molec, used in this study), and thus a larger vibrational population.

Using standard values for the α parameters for the neutral dissociation reactions and for the activation energy of dissociation of CO_2 upon impact with O atoms, our model predicts a CO_2 conversion and energy efficiency up to 32% and 47%, respectively, for a gas temperature of 300 K, an ionization degree of 10^{-4}, and a very low reduced electric field (10 Td). At 50 Td, the corresponding values are 30% and 43%, respectively. At ionization degrees typical of gliding arc and microwave discharges (i.e. around 10^{-6}), a maximum conversion and energy efficiency of 29% and 42%, are reached, respectively, for a reduced electric field of 45 Td and a gas temperature of 300 K. Plasma can still be sustained at this low E/N, as e.g. shown experimentally in a glow discharge by Andreev et al. [60].

Furthermore, we identified that the vibrational energy consumption of dissociation is a strong limitation to the energy efficiency. Indeed, the activation energy of the dissociation of CO_2 upon collision with an O atom is quite high (we considered a value of 2.25 eV in this study), while the enthalpy of the reaction is significantly lower (0.35 eV at standard conditions). Moreover, the vibrational energy only has a limited efficiency to overcome the activation energy barrier of this reaction. It thus requires an energy $E_a(N2)/\alpha_O$ to overcome the barrier. Therefore, the vibrational energy required to overcome the activation energy barrier is high and the excess energy is typically wasted to heat.

By varying the parameters α of the two main dissociation reactions (i.e. upon collision with any neutral molecule, or upon collision with O atoms), we can increase the conversion and energy efficiency up to 62% (at $E/N = 50$ Td, 300 K and an ionization degree of 10^{-5}). Furthermore, by varying the parameter α as well as the activation energy of the dissociation upon collision with an O atom, the conversion and energy efficiency can be further increased up to 72%. Using the most optimal values of activation energy and α, as well as plasma operating conditions ($E/N = 10$ Td, 300 K and an ionization degree of 10^{-4}), the model predicts an energy efficiency up to 86%. The fact that this is not 100% is attributed to other losses in the kinetics of CO_2 conversion, more specifically the fact that still not all electron energy will go to vibrational excitation of CO_2, but some fraction is also spent to the dissociation products (CO and O_2).

Finally, we derived an empirical expression for the theoretical maximum energy efficiency that can be reached by this model, given certain values for the activation energy and α parameters of the two neutral dissociation reactions. This formula can be used to identify the theoretical limitations to the energy efficiency, based on a given set of rate coefficients. Using the most optimal values of activation energy and α, a theoretical maximum energy efficiency of 100% is predicted.

Using the activation energies (and thus rate coefficients) and the α values adopted from literature, a theoretical maximum energy efficiency of 58% was reached. Comparing this value with the actual values predicted by the model, with a maximum of 47%, shows that a very low E/N (10 Td), low gas temperature (300 K) and a high ionization degree (10^{-4}) are nearly ideal for the most energy efficient CO_2 conversion. The most common discharges used for CO_2 conversion operate at clearly different conditions, i.e. somewhat higher E/N (50–100 Td), higher gas temperature (up to a few 1000 K) and lower ionization degree (10^{-6}) for MW and GA discharges, and significantly higher E/N (200 Td and above) for DBDs. This indicates that there is clearly room for optimization of the most common discharges used for CO_2 conversion, by modifying the setups, or developing new devices, working simultaneously at low E/N, gas temperatures close to room temperature and high ionization degrees.

Conflict of interest

None declared.

Acknowledgements

We acknowledge financial support from the European Union's Seventh Framework Program for research, technological development and demonstration under grant agreement no. 606889. The calculations were carried out using the Turing HPC infrastructure at the CalcUA core facility of the Universiteit Antwerpen (UA), a division of the Flemish Supercomputer Center VSC, funded by the Hercules Foundation, the Flemish Government (department EWI) and the UA. We would also like to thank Prof. Richard van de Sanden (DIFFER) for the interesting talks.

Appendix A. Appendix

This appendix lists all the chemical reactions included in the model, as well as the rate coefficients and the references where these data are adopted from.

Table A.1
Electron impact reactions calculated with cross sections data, using the calculated EEDF, as explained in Section 2.1 of the main paper, as well as the references where the data are adopted from.

No.	Reaction	Reference	Note
(X1)[a]	$e + CO_2 \rightarrow 2e + CO_2^+$	[58]	
(X2)[b]	$e + CO_2 \rightarrow 2e + O + CO^+$	[58]	
(X3)[b]	$e + CO_2 \rightarrow O^- + CO$	[58]	
(X4)[b]	$e + CO_2 \rightarrow e + O + CO$	[58]	
(X5)[a]	$e + CO_2 \rightarrow e + CO_2^*$	[58]	
(X6)[c]	$e + CO_2 \rightarrow e + CO_2v_x$	[58]	$x = a, b, c, d$
(X7)[c]	$e + CO_2v_i \rightarrow e + CO_2v_j$	[58]	
(X8)[b]	$e + CO \rightarrow 2e + CO^+$	[69]	
(X9)[b]	$e + CO \rightarrow C + O^-$	[70]	
(X9bis)[b]	$e + CO \rightarrow e + C + O$	[71]	
(X10)[a]	$e + CO \rightarrow e + CO(E_x)$	[71]	x = 1–4
(X11)[c]	$e + CO \rightarrow e + COv_i$	[71]	i = 1–5
(X12)[b]	$e + O_2 \rightarrow e + O + O$	[72]	
(X12M)[a]	$e + O_2 + M \rightarrow e + O_2^- + M$	[72]	
(X13)[b]	$e + O_2 \rightarrow O + O^-$	[72]	
(X14)[c]	$e + O_2 \leftrightarrow e + O_2v_i$	[72]	i = 1, 2, 3
(X17)[a]	$e + O_2 \leftrightarrow e + O_2E_i$	[72]	i = 1, 2

[a] Same cross-section also used for CO_2v_i (i = the various vibrationally excited levels).
[b] Cross-section also used for CO_2v_i, modified by lowering the energy threshold by the energy of the excited state of CO_2v_i.
[c] Cross-section for the various levels (i, j) scaled and shifted using Fridman's approximation from the ($0 \rightarrow 1$) cross-section.

Table A.2
Electron impact reactions using analytical expressions for the rate coefficients, given in m^3/s and m^6/s, for two-body and three-body reactions, respectively, as well as the references where the data are adopted from. T_g and T_e are given in K and eV, respectively.

No.	Reaction	Rate coefficient	Reference
(E1a)	$e + CO_2^+ \rightarrow CO(v_1) + O$	$(1 - \beta_{E1}) \times 2.0 \times 10^{-11} T_e^{-0.5} T_g^{-1}$	[73,74]
(E1b)	$e + CO_2^+ \rightarrow C + O_2$	$\beta_{E1} \times k_{E1a} = \frac{k_{E1a}}{2}$	[75]
(E2)[a]	$e + CO_4^+ \rightarrow CO_2 + O_2$	$1.61 \times 10^{-13} T_e^{-0.5}$	[75]
(E3)	$e + CO^+ \rightarrow C + O$	$3.46 \times 10^{-14} T_e^{-0.48}$	[76,77]
(E4)[a]	$e + O + M \rightarrow O^- + M$	1×10^{-43}	[74]

[a] The primary source was not accessible and/or the uncertainty was not given.

Table A.3
Ion-ion and ion-neutral reactions, as well as the references where the data are adopted from. The rate coefficients are given in m^3/s and m^6/s, for two-body and three-body reactions, respectively. T_g is given in K.

No.	Reaction	Rate coefficient	Reference
(I1)	$CO_2 + CO^+ \rightarrow CO_2^+ + CO$	1.0×10^{-15}	[78,79]
(I2a)[b]	$CO_2 + O^- + CO_2 \rightarrow CO_3^- + CO_2$	1.5×10^{-40}	[78,80]
(I2b)[b]	$CO_2 + O^- + CO \rightarrow CO_3^- + CO$	1.5×10^{-40}	[78,80]
(I2c)	$CO_2 + O^- + O_2 \rightarrow CO_3^- + O_2$	3.1×10^{-40}	[78,80]
(I3)	$CO_2 + O_2^- + M \rightarrow CO_4^- + M$	4.7×10^{-41}	[78,80]
(I4)	$CO + O^- \rightarrow CO_2 + e$	5.5×10^{-16}	[78,81]
(I5)	$CO + CO_3^- \rightarrow 2CO_2 + e$	5×10^{-19}	[82]
(I6)[a]	$CO_3^- + CO_2^+ \rightarrow 2CO_2v_b + O$	5×10^{-13}	[74]
(I7)[a]	$CO_4^- + CO_2^+ \rightarrow 2CO_2v_b + O_2$	5×10^{-13}	[74]
(I8)[a]	$O_2^- + CO_2^+ \rightarrow CO_2v_1 + O_2 + O$	6×10^{-13}	[74]
(I9)	$CO_3^- + O \rightarrow CO_2 + O_2^-$	8×10^{-17}	[83]
(I10a)[a]	$CO_4^- + O \rightarrow CO_3^- + O_2 + O$	1.12×10^{-16}	[78]
(I10b)[a]	$CO_4^- + O \rightarrow CO_2 + O_2 + O^-$	1.4×10^{-17}	[78]
(I11)	$O + O^- \rightarrow O_2 + e$	2.3×10^{-16}	[84]
(I12)[a]	$O + O_2^- \rightarrow O_2 + O^-$	1.5×10^{-16}	[78]
(I13)	$O_2^- + M \rightarrow O_2 + M + e$	$2.7 \times 10^{-16} \left(\frac{T_g}{300}\right)^{0.5} \exp(-5590/T_g)$	[85,86]
(I14)[c]	$O^- + M \rightarrow O + M + e$	$2.3 \times 10^{-15} \exp(-26000/T_g)$	[87,88,86]

[a] The primary source was not accessible and/or the uncertainty was not given.
[b] The rate coefficient of $CO_2 + O^- + He \rightarrow CO_3^- + He$ was used, due to the lack of further information.
[c] For usual values of gas temperature, i.e. $T_g \ll 26{,}000$ K, the rate coefficient is very low, as pointed out by Gudmundsson [89].

Table A.4
Neutral-neutral reactions, as well as the references where the data are adopted from. The rate coefficients are given in m^3/s and m^6/s, for two-body and three-body reactions, respectively. T_g is given in K. The α parameter determines the effectiveness of lowering the activation energy for reaction involving vibrationally excited levels of the molecules.

No.	Reaction	Rate coefficient	α	References
(N1)	$CO_2 + M \rightarrow CO + O + M$	$6.06 \times 10^{-16} \exp(-52525/T_g)$	0.82 or α_M	[90]
(N2)	$CO_2 + O \rightarrow CO + O_2$	$2.8 \times 10^{-17} \exp(-26500/T_g)$	0.5 or α_O	[65,91]
(N3)	$CO_2 + C \rightarrow 2CO$	$< 10^{-21}$	n.a.	[92]
(N4)[a]	$CO + O + M \rightarrow CO_2 + M$	$8.3 \times 10^{-46} \exp(-1510/T_g)$	0.0	[93,91]
(N5)	$O_2 + CO \rightarrow CO_2 + O$	$4.2 \times 10^{-18} \exp(-24000/T_g)$	0.5	[91]
(N6)	$O_2 + C \rightarrow CO + O$	$1.99 \times 10^{-16} \exp(-2010/T_g)$	0.0	[94]
(N7)	$O + C + M \rightarrow CO + M$	$2.14 \times 10^{-41} \left(\frac{T_g}{300}\right)^{-3.08} \exp(-2144/T_g)$	n.a.	[65,91]
(N8)	$O + O + M \rightarrow O_2 + M$	$5.2 \times 10^{-47} \exp(900/T_g)$	n.a.	[65,91]
(N9)	$O_2 + M \rightarrow O + O + M$	$3.0 \times 10^{-12} \frac{1}{T_g} \exp(-59380/T_g)$	0.0	[65,91]

[a] Multiply by 7, 3 or 12 for M = CO_2, CO or O_2 respectively.

Table A.5
Neutral reactions between vibrationally excited molecules, as well as the references where the data are adopted from. The rate coefficients are given in m^3/s and m^6/s, for two-body and three-body reactions, respectively. T_g is given in K. Reverse reactions are included via detailed balancing.

No.	Reaction	Rate coefficient	References
(V1)	$CO_2v_a + M \leftrightarrow CO_2 + M$	$7.14 \times 10^{-15} \exp(-177T_g^{-1/3} + 451T_g^{-2/3})$	[95–97]
(V2a)	$CO_2v_1 + M \leftrightarrow CO_2v_a + M$	$4.25 \times 10^{-7} \exp(-407T_g^{-1/3} + 824T_g^{-2/3})$	[98,99,97]
(V2b)	$CO_2v_1 + M \leftrightarrow CO_2v_b + M$	$8.57 \times 10^{-7} \exp(-404T_g^{-1/3} + 1096T_g^{-2/3})$	[98,99,97]
(V2c)	$CO_2v_1 + M \leftrightarrow CO_2v_c + M$	$1.43 \times 10^{-7} \exp(-252T_g^{-1/3} + 685T_g^{-2/3})$	[98,99,97]
(V3)	$COv_1 + M \leftrightarrow CO + M$	$1.0 \times 10^{-18} T_g \exp(-150.7T_g^{-1/3})$	[51]
(V4)	$O_2v_1 + M \leftrightarrow O_2 + M$	$1.3 \times 10^{-14} \exp(-158.7T_g^{-1/3})$	[96,97]
(V5)	$CO_2v_1 + CO_2 \leftrightarrow CO_2v_a + CO_2v_b$	$1.06 \times 10^{-11} \exp(-242T_g^{-1/3} + 633T_g^{-2/3})$	[98,99,97]
(V6)	$CO_2v_1 + CO_2 \leftrightarrow CO_2 + CO_2v_1$	$1.32 \times 10^{-18} \left(\frac{T_g}{300}\right)^{0.5} \frac{250}{T_g}$	[100,101]
(V7)	$COv_1 + CO \leftrightarrow CO + COv_1$	$3.4 \times 10^{-16} \left(\frac{T_g}{300}\right)^{0.5} \left(1.64 \times 10^{-6} T_g + \frac{1.61}{T_g}\right)$	[102,103]
(V8)	$CO_2v_1 + CO \leftrightarrow CO_2 + COv_1$	$4.8 \times 10^{-12} \exp(-153T_g^{-1/3})$	[104,97]

References

[1] IPCC, Fifth Assessment Report: Climate Change Synthesis Report, (2013) https://www.ipcc.ch/pdf/assessment-report/ar5/syr/AR5_SYR_FINAL_SPM.pdf.
[2] R. Snoeckx, A. Bogaerts, Plasma technology: a novel solution for CO_2 conversion? Chem. Soc. Rev. 46 (2017) 5805–5863.
[3] J.A. Martens, A. Bogaerts, N. De Kimpe, P.A. Jacobs, G.B. Marin, K. Rabaey, M. Saeys, S. Verhelst, The chemical route to a carbon dioxide neutral world, ChemSusChem 10 (2017) 1039–1055.
[4] G.J. van Rooij, H.N. Akse, W.A. Bongers, M.C.M. van de Sanden, Plasma for electrification of chemical industry: a case study on CO_2 reduction, Plasma Phys. Control. Fusion 60 (2018) 014019.
[5] A. Fridman, Plasma Chemistry, Cambridge University Press, New York, 2008.
[6] R.I. Asisov, A.K. Vakar, V.K. Jivotov, M.F. Krotov, O.A. Zinoviev, B.V. Potapkin, A.A. Rusanov, V.D. Rusanov, A.A. Fridman, Non-equilibrium plasma-chemical process of CO_2 decomposition in a supersonic microwave discharge, Proc. USSR Acad. Sci. 27 (1983).
[7] L.F. Spencer, A.D. Gallimore, CO_2 dissociation in an atmospheric pressure plasma/catalyst system: a study of efficiency, Plasma Sources Sci. Technol. 22 (2012) 015019.
[8] T. Silva, N. Britun, T. Godfroid, R. Snyders, Optical characterization of a microwave pulsed discharge used for dissociation of CO_2, Plasma Sources Sci. Technol. 23 (2014) 025009.
[9] W. Bongers, H. Bouwmeester, B. Wolf, F. Peeters, S. Welzel, D. van den Bekerom, N. den Harder, A. Goede, M. Graswinckel, P.W. Groen, J. Kopecki, M. Leins, G. van Rooij, A. Schulz, M. Walker, R. van de Sanden, Plasma-driven dissociation of CO_2 for fuel synthesis, Plasma Process. Polym. 14 (2017) 1600126.
[10] N. den Harder, D.C.M. van den Bekerom, R.S. Al, M.F. Graswinckel, J.M. Palomares, F.J.J. Peeters, S. Ponduri, T. Minea, W.A. Bongers, M.C.M. van de Sanden, G.J. van Rooij, Homogeneous CO_2 conversion by microwave plasma: wave propagation and diagnostics, Plasma Process. Polym. 14 (2017) 1600120.
[11] A. Indarto, D.R. Yang, J.W. Choi, H. Lee, H.K. Song, Gliding arc plasma processing of CO_2 conversion, J. Hazard. Mater. 146 (2007) 309–315.
[12] T. Nunnally, K. Gutsol, A. Rabinovich, A. Fridman, A. Gutsol, A. Kemoun, Dissociation of CO_2 in a low current gliding arc plasmatron, J. Phys. D: Appl. Phys. 44 (2011) 274009.
[13] M. Ramakers, G. Trenchev, S. Heijkers, W. Wang, A. Bogaerts, Gliding arc plasmatron: providing an alternative method for carbon dioxide conversion, ChemSusChem 10 (2017) 2642–2652.
[14] D. Mei, X. Zhu, Y.-L. He, J.D. Yan, X. Tu, Plasma-assisted conversion of CO_2 in a dielectric barrier discharge reactor: understanding the effect of packing materials, Plasma Sources Sci. Technol. 24 (2015) 15011–15021.
[15] S. Paulussen, B. Verheyde, X. Tu, C. De Bie, T. Martens, D. Petrovic, A. Bogaerts, B. Sels, Conversion of carbon dioxide to value-added chemicals in atmospheric pressure dielectric barrier discharges, Plasma Sources Sci. Technol. 19 (2010) 034015.
[16] I. Belov, S. Paulussen, A. Bogaerts, Appearance of a conductive carbonaceous coating in a CO_2 dielectric barrier discharge and its influence on the electrical properties and the conversion efficiency, Plasma Sources Sci. Technol. 25 (2016) 015023.
[17] I. Michielsen, Y. Uytdenhouwen, J. Pype, B. Michielsen, J. Mertens, F. Reniers, V. Meynen, A. Bogaerts, CO_2 dissociation in a packed bed DBD reactor: first steps towards a better understanding of plasma catalysis, Chem. Eng. J. 326 (2017) 477–488.
[18] M.S. Moss, K. Yanallah, R.W.K. Allen, F. Pontiga, An investigation of CO_2 splitting using nanosecond pulsed corona discharge: effect of argon addition on CO_2 conversion and energy efficiency, Plasma Sources Sci. Technol. 26 (2017) 035009.
[19] M. Scapinello, L.M. Martini, G. Dilecce, P. Tosi, Conversion of CH_4/CO_2 by a nanosecond repetitively pulsed discharge, J. Phys. D: Appl. Phys. 49 (2016) 075602.
[20] V. Shapoval, E. Marotta, C. Ceretta, N. Konjević, M. Ivković, M. Schiorlin, C. Paradisi, Development and testing of a self-triggered spark reactor for plasma driven dry reforming of methane, Plasma Process. Polym. 11 (2014) 787–797.
[21] J.-y. Wang, G.-g. Xia, A. Huang, S.L. Suib, Y. Hayashi, H. Matsumoto, CO_2

decomposition using glow discharge plasmas, J. Catal. 185 (1999) 152–159.
[22] T. Kozák, A. Bogaerts, Evaluation of the energy efficiency of CO_2 conversion in microwave discharges using a reaction kinetics model, Plasma Sources Sci. Technol. 24 (2015) 015024.
[23] A. Bogaerts, T. Kozák, K. van Laer, R. Snoeckx, Plasma-based conversion of CO_2: current status and future challenges, Farad. Discuss. 183 (2015) 217–232.
[24] A. Bogaerts, C. De Bie, R. Snoeckx, T. Kozák, Plasma based CO_2 and CH_4 conversion: a modeling perspective, Plasma Process. Polym. 14 (2017) e201600070.
[25] M. Capitelli, Nonequilibrium Vibrational Kinetics. Vol. 39 of Topics in Current Physics, Springer, Berlin, Heidelberg, 1986, http://dx.doi.org/10.1007/978-3-642-48615-9.
[26] A. Berthelot, A. Bogaerts, Modeling of CO_2 splitting in a microwave plasma: how to improve the conversion and energy efficiency, J. Phys. Chem. C 121 (2017) 8236–8251.
[27] S. Heijkers, A. Bogaerts, CO_2 conversion in a gliding arc plasmatron: elucidating the chemistry through kinetic modeling, J. Phys. Chem. C 121 (2017) 22644–22655.
[28] L.D. Pietanza, G. Colonna, G. D'Ammando, A. Laricchiuta, M. Capitelli, Vibrational excitation and dissociation mechanisms of CO_2 under non-equilibrium discharge and post-discharge conditions, Plasma Sources Sci. Technol. 24 (2015) 042002.
[29] L.D. Pietanza, G. Colonna, G. D'Ammando, A. Laricchiuta, M. Capitelli, Electron energy distribution functions and fractional power transfer in "cold" and excited CO_2 discharge and post discharge conditions, Phys. Plasmas 23 (2016).
[30] L.D. Pietanza, G. Colonna, G. D'Ammando, A. Laricchiuta, M. Capitelli, Non-equilibrium vibrational assisted dissociation and ionization mechanisms in cold CO_2 plasmas, Chem. Phys. 468 (2016) 44–52.
[31] L.D. Pietanza, G. Colonna, V. Laporta, R. Celiberto, G. D'Ammando, A. Laricchiuta, M. Capitelli, Influence of electron molecule resonant vibrational collisions over the symmetric mode and direct excitation-dissociation cross sections of CO_2 on the electron energy distribution function and dissociation mechanisms in cold pure CO_2 plasmas, J. Phys. Chem. A 120 (2016) 2614–2628.
[32] L.D. Pietanza, G. Colonna, G. D'Ammando, M. Capitelli, Time-dependent coupling of electron energy distribution function, vibrational kinetics of the asymmetric mode of CO_2 and dissociation, ionization and electronic excitation kinetics under discharge and post-discharge conditions, Plasma Phys. Control. Fusion 59 (2017) 014035.
[33] M. Capitelli, G. Colonna, G. D'Ammando, K. Hassouni, A. Laricchiuta, L.D. Pietanza, Coupling of plasma chemistry, vibrational kinetics, collisional-radiative models and electron energy distribution function under non-equilibrium conditions, Plasma Process. Polym. 14 (2017) 1600109.
[34] L.D. Pietanza, G. Colonna, M. Capitelli, Non-equilibrium plasma kinetics of reacting CO: an improved state to state approach, Plasma Sources Sci. Technol. (2017) Accepted manuscript.
[35] R. Aerts, T. Martens, A. Bogaerts, Influence of vibrational states on CO_2 splitting by dielectric barrier discharges, J. Phys. Chem. C 116 (2012) 23257–23273.
[36] T. Kozák, A. Bogaerts, Splitting of CO_2 by vibrational excitation in non-equilibrium plasmas: a reaction kinetics model, Plasma Sources Sci. Technol. 23 (2014) 045004.
[37] A. Berthelot, A. Bogaerts, Modeling of plasma-based CO_2 conversion: lumping of the vibrational levels, Plasma Sources Sci. Technol. 25 (2016) 045022.
[38] W. Wang, A. Berthelot, S. Kolev, X. Tu, A. Bogaerts, CO_2 conversion in a gliding arc plasma: 1D cylindrical discharge model, Plasma Sources Sci. Technol. 25 (2016) 065012.
[39] S. Sun, H. Wang, D. Mei, X. Tu, A. Bogaerts, CO_2 conversion in a gliding arc plasma: performance improvement based on chemical reaction modeling, J. CO_2 Util. 17 (2017) 220–234.
[40] S. Ponduri, M.M. Becker, S. Welzel, M.C.M. Van De Sanden, D. Loffhagen, R. Engeln, Fluid modelling of CO_2 dissociation in a dielectric barrier discharge, J. Appl. Phys. 119 (2016).
[41] M. Grofulović, L.L. Alves, V. Guerra, Electron-neutral scattering cross sections for CO_2: a complete and consistent set and an assessment of dissociation, J. Phys. D: Appl. Phys. 49 (2016) 395207.
[42] A. Bogaerts, W. Wang, A. Berthelot, V. Guerra, Modeling plasma-based CO_2 conversion: crucial role of the dissociation cross section, Plasma Sources Sci. Technol. 25 (2016) 055016.
[43] M.M. Turner, Uncertainty and error in complex plasma chemistry models, Plasma Sources Sci. Technol. 24 (2015) 035027.
[44] M.M. Turner, Uncertainty and sensitivity analysis in complex plasma chemistry models, Plasma Sources Sci. Technol. 25 (2016) 015003.
[45] M.M. Turner, Computer simulation in low-temperature plasma physics: future challenges, Plasma Process. Polym. (2016) 201600121.
[46] P. Koelman, S. Heijkers, S. Tadayon Mousavi, W. Graef, D. Mihailova, T. Kozak, A. Bogaerts, J. van Dijk, A comprehensive chemical model for the splitting of CO_2 in non-equilibrium plasmas, Plasma Process. Polym. 14 (2017) 1600155.
[47] A. Berthelot, A. Bogaerts, Modeling of CO_2 plasma: effect of uncertainties in the plasma chemistry, Plasma Sources Sci. Technol. 26 (2017) 115002.
[48] NIST Chemistry WebBook, NIST Standard Reference Database Number 69 Constants of Diatomic Molecules. Retrieved 5 June 2017: http://webbook.nist.gov.
[49] G.H.K.P. Huber, Molecular Spectra and Molecular Structure IV. Constant of diatomic molecules, Van Nostrand Rienhold Company, 1979.
[50] R.N. Schwartz, Z.I. Slawsky, K.F. Herzfeld, Calculation of vibrational relaxation times in gases, J. Chem. Phys. 20 (1952) 1591.
[51] M. Capitelli, C.M. Ferreira, B.F. Gordiets, A.I. Osipov, Plasma Kinetics in Atmospheric Gases, Springer Berlin Heidelberg, 2000.
[52] R.D. Levine, R.B. Bernstein, Thermodynamic Approach to Collision Processes, Springer US, Boston, MA, 1976, pp. 323–364, http://dx.doi.org/10.1007/978-1-4757-0644-4_7.
[53] S. Pancheshnyi, B. Eismann, G.J.M. Hagelaar, L.C. Pitchford, Computer Code ZDPlasKin, University of Toulouse, LAPLACE, CNRS-UPS-INP, Toulouse, France, 2008http://www.zdplaskin.laplace.univ-tlse.fr.
[54] P.N. Brown, G.D. Byrne, A.C. Hindmarsh, VODE: a variable-coefficient ODE solver, SIAM J. Sci. Stat. Comput. 10 (1989) 1038–1051.
[55] G.J.M. Hagelaar, L.C. Pitchford, Solving the Boltzmann equation to obtain electron transport coefficients and rate coefficients for fluid models, Plasma Sources Sci. Technol. 14 (2005) 722–733.
[56] W. Wang, D. Mei, X. Tu, A. Bogaerts, Gliding arc plasma for CO_2 conversion: better insights by a combined experimental and modelling approach, Chem. Eng. J. 330 (2017) 11–25.
[57] N. Pinhão, A. Moura, J. Branco, J. Neves, Influence of gas expansion on process parameters in non-thermal plasma plug-flow reactors: a study applied to dry reforming of methane, Int. J. Hydrogen Energy 41 (2016) 9245–9255.
[58] A.V. Phelps, Phelps Database, (2014) Retrieved from www.lxcat.net, http://jilawww.colorado.edu/ avp/.
[59] W. Wang, A. Bogaerts, Effective ionisation coefficients and critical breakdown electric field of CO_2 at elevated temperature: effect of excited states and ion kinetics, Plasma Sources Sci. Technol. 25 (2016) 055025.
[60] S. Andreev, V. Zakharov, V. Ochkin, S. Savinov, Plasma-chemical CO_2 decomposition in a non-self-sustained discharge with a controlled electronic component of plasma, Spectrochim. Acta Part A: Mol. Biomol. Spectrosc. 60 (2004) 3361–3369.
[61] R. Aerts, W. Somers, A. Bogaerts, Carbon dioxide splitting in a dielectric barrier discharge plasma: a combined experimental and computational study, ChemSusChem 8 (2015) 702–716.
[62] A. Ozkan, A. Bogaerts, F. Reniers, Routes to increase the conversion and the energy efficiency in the splitting of CO_2 by a dielectric barrier discharge, J. Phys. D: Appl. Phys. 50 (2017) 084004.
[63] C.E. Treanor, J.W. Rich, R.G. Rehm, Vibrational relaxation of anharmonic oscillators with exchange-dominated collisions, J. Chem. Phys. 48 (1968) 1798–1807.
[64] P. Diomede, M.C.M. van de Sanden, S. Longo, Insight into CO_2 dissociation in plasma from numerical solution of a vibrational diffusion equation, J. Phys. Chem. C 121 (2017) 19568–19576.
[65] D.L. Baulch, D.D. Drysdale, J. Duxbury, S. Grant, Evaluated Kinetic Data for High Temperature Reactions. Volume 3: Homogeneous Gas Phase Reactions of the O_2–O_3 System, The CO–O_2–H_2 System, and of the Sulphur-Containing Species, Butterworth, London, 1976.
[66] G. Chen, N. Britun, T. Godfroid, V. Georgieva, R. Snyders, M.-P. Delplancke-Ogletree, An overview of CO_2 conversion in a microwave discharge: the role of plasma-catalysis, J. Phys. D: Appl. Phys. 50 (2017) 084001.
[67] J.C. Whitehead, Plasma-catalysis: the known knowns, the known unknowns and the unknown unknowns, J. Phys. D: Appl. Phys. 49 (2016) 243001.
[68] E.C. Neyts, K.K. Ostrikov, M.K. Sunkara, A. Bogaerts, Plasma catalysis: synergistic effects at the nanoscale, Chem. Rev. 115 (2015) 13408–13446.
[69] C. Tian, C.R. Vidal, Cross sections of the electron impact dissociative ionization of CO, CH_4 and C_2H_2, J. Phys. B: At. Mol. Opt. Phys. 31 (1998) 895–909.
[70] D. Rapp, D.D. Briglia, Total cross sections for ionization and attachment in gases by electron impact. II. Negative ion formation, J. Chem. Phys. 43 (1965) 1480–1489.
[71] J.E. Land, Electron scattering cross sections for momentum transfer and inelastic excitation in carbon monoxide, J. Appl. Phys. 49 (1978) 5716–5721.
[72] S.A. Lawton, A.V. Phelps, Excitation of the b $^1\Sigma_g^+$ state of O_2 by low energy electrons, J. Chem. Phys. 69 (1978) 1055.
[73] C.S. Weller, M.A. Biondi, Measurements of dissociative recombination of CO^{2+} ions with electrons, Phys. Rev. Lett. 19 (1967) 59–61.
[74] J. Thoenes, S.C. Kurzius, Plasma Chemistry Processes in the Closed Cycle EDL – Technical Report DRCPM-HEL-CR-79-11-VOL-1, Technical Report, Lockheed Missiles and Space Co Inc., Huntsville AL, 1979.
[75] T.G. Beuthe, J.-S. Chang, Chemical kinetic modelling of non-equilibrium Ar–CO_2 thermal plasmas, Jap. J. Appl. Phys. 36 (1997) 4997–5002.
[76] J.B.A. Mitchell, H. Hus, The dissociative recombination and excitation of CO^+, J. Phys. B: At. Mol. Phys. 18 (1985) 547–555.
[77] D. Mcelroy, C. Walsh, A.J. Markwick, M.A. Cordiner, K. Smith, T.J. Millar, The UMIST database for astrochemistry 2012, Astron. Astrophys. 550 (2013).
[78] D. Albritton, Ion-neutral reaction-rate constants measured in flow reactors through 1977, At. Data Nucl. Data Tables 22 (1978) 1–101.
[79] N. Adams, D. Smith, D. Grief, Reactions of H_nCO^+ ions with molecules at 300 K, Int. J. Mass Spectrom. Ion Phys. 26 (1978) 405–415.
[80] F.C. Fehsenfeld, E.E. Ferguson, Laboratory studies of negative ion reactions with atmospheric trace constituents, J. Chem. Phys. 61 (1974) 3181–3193.
[81] M. Mcfarland, D.L. Albritton, F.C. Fehsenfeld, E.E. Ferguson, A.L. Schmeltekopf, Flow-drift technique for ion mobility and ion-molecule reaction rate constant measurements. III. Negative ion reactions of O^- with CO, NO, H_2, and D_2, J. Chem. Phys. 59 (1973) 6629–6635.
[82] D. Price, J. Moruzzi, Negative ion molecule reactions in CO_2 at high pressures and temperatures, Vacuum 24 (1974) 591–593.
[83] F.C. Fehsenfeld, A.L. Schmeltekopf, H.I. Schiff, E.E. Ferguson, Laboratory measurements of negative ion reactions of atmospheric interest, Planet. Space Sci. 15 (1967) 373–379.
[84] S.G. Belostotsky, D.J. Economou, D.V. Lopaev, T.V. Rakhimova, Negative ion destruction by $O(^3P)$ atoms and $O_2(a^1\Delta_g)$ molecules in an oxygen plasma, Plasma Sources Sci. Technol. 14 (2005) 532–542.
[85] J.L. Pack, A.V. Phelps, Electron attachment and detachment. II. Mixtures of O_2 and

CO_2 and of O_2 and H_2O, J. Chem. Phys. 45 (1966) 4316–4329.
[86] M.H. Bortner, T. Bourer, C.A. Blank, Defense Nuclear Agency Reaction Rate Handbook, 2nd ed. AD 763699, Technical Report, (1972).
[87] J.B. Hasted, R.A. Smith, The detachment of electrons from negative ions, Proc. R. Soc. A: Math. Phys. Eng. Sci. 235 (1956) 349–353.
[88] L. Frommhold, Über verzögerte Elektronen in Elektronenlawinen, insbesondere in Sauerstoff und Luft, durch Bildung und Zerfall negativer Ionen (O^-), Fortsch. Phys. 12 (1964) 597–642.
[89] J.T. Gudmundsson, A Critical Review of the Reaction Set for a Low Pressure Oxygen Processing Discharge RH-17-2004, Technical Report, University of Iceland, 2004.
[90] M. Burmeister, P. Roth, ARAS measurements on the thermal decomposition of CO_2 behind shock waves, AIAA J. 28 (1990) 402–405.
[91] W. Tsang, R.F. Hampson, Chemical kinetic data base for combustion chemistry. Part I. Methane and related compounds, J. Phys. Chem. Ref. Data 15 (1986) 1087–1279.
[92] D. Husain, A.N. Young, Kinetic investigation of ground state carbon atoms, $C(2^3P_J)$, J. Chem. Soc., Farad. Trans. 2 (71) (1975) 525.
[93] R.R. Baldwin, D. Jackson, A. Melvin, B.N. Rossiter, The second limit of hydrogen + carbon monoxide + oxygen mixtures, Int. J. Chem. Kinet. 4 (1972) 277–292.
[94] A.J. Dean, D.F. Davidson, R.K. Hanson, A shock tube study of reactions of carbon atoms with hydrogen and oxygen using excimer photolysis of C_3O_2 and carbon atom atomic resonance absorption spectroscopy, J. Phys. Chem. 95 (1991) 183–191.
[95] C.J.S.M. Simpson, T.R.D. Chandler, A.C. Strawson, Vibrational relaxation in CO_2 and CO_2–Ar mixtures studied using a shock tube and a laser-Schlieren technique, J. Chem. Phys. 51 (1969) 2214–2219.
[96] R. Taylor, S. Bitterman, Survey of vibrational relaxation data for processes important in the CO_2–N_2 laser system, Rev. Mod. Phys. 41 (1969) 26–47.
[97] J.A. Blauer, G.R. Gilmore, A Survey of Vibrational Relaxation Rate Data for Processes Important to CO_2–N_2–H_2O Infrared Plume Radiation, Technical Report, Ultrasystems, Inc., 1973 afrpl-tr-7.
[98] W.A. Rosser, A.D. Wood, E.T. Gerry, Deactivation of vibrationally excited carbon dioxide (ν_3) by collisions with carbon dioxide or with nitrogen, J. Chem. Phys. 50 (1969) 4996–5008.
[99] K.F. Herzfeld, Deactivation of vibrations by collision in the presence of Fermi resonance, J. Chem. Phys. 47 (1967) 743–752.
[100] R.D. Sharma, Near resonant vibrational energy transfer among isotopes of CO_2, Phys. Rev. 177 (1969) 102–107.
[101] T.G. Kreutz, J.A. O'Neill, G.W. Flynn, Diode laser absorption probe of vibration-vibration energy transfer in CO_2, J. Phys. Chem. 91 (1987) 5540–5543.
[102] R.L. DeLeon, J. Rich, Vibrational energy exchange rates in carbon monoxide, Chem. Phys. 107 (1986) 283–292.
[103] C. Flament, T. George, K.A. Meister, J.C. Tufts, J.W. Rich, V.V. Subramaniam, J.P. Martin, B. Piar, M.Y. Perrin, Nonequilibrium vibrational kinetics of carbon monoxide at high translational mode temperatures, Chem. Phys. 163 (1992) 241–262.
[104] W.A. Rosser, R.D. Sharma, E.T. Gerry, Deactivation of vibrationally excited carbon dioxide (001) by collisions with carbon monoxide, J. Chem. Phys. 54 (1971) 1196–1205.